Pisias, N.G., Mayer, L.A., Janecek, T.R., Palmer-Julson, A., and van Andel, T.H. (Eds.), 1995
Proceedings of the Ocean Drilling Program, Scientific Results, Vol. 138

18. ESTIMATING LITHOLOGY FROM NONINTRUSIVE REFLECTANCE SPECTRA: LEG 138[1]

Alan C. Mix,[2] Sara E. Harris,[2] and Thomas R. Janecek[3]

ABSTRACT

During Leg 138, we measured reflectance spectra in the visible and near-infrared bands (455–945 nm) every few centimeters on split core surfaces from eastern tropical Pacific Ocean sediments. Here, we evaluate predictions of the content of biogenic calcite, biogenic opal, and nonbiogenic sediments from the reflectance spectra. For Sites 844 through 847, which contain a significant nonbiogenic component, reflectance spectra yielded a useful proxy for the percentages of $CaCO_3$ over a wide range of values from nearly 0% to 100%, with root-mean-square (RMS) errors of about 9%. Direct estimates of "nonbiogenic" sediment percentages, approximated by 100 – ($CaCO_3$ + opal), were reasonably successful (RMS error of 10%), however, were incorrect in some intervals. This suggests that mineralogy of the nonbiogenic material changes through time and that further subdivision of this component will be needed for useful estimation from reflectance. For percentages of biogenic opal, calibration equations appear to work well (RMS error of 6%) at concentrations of less than 30%, but for higher opal concentrations, reflectance equations often underestimate the true contents of opal. Improvements in multiparameter lithologic estimates from reflectance spectra may come from (1) expanding the wavelengths measured to better capture unique mineral reflectance bands, and (2) adding the ability to measure diffuse, rather than directional, reflectance to minimize the effects of surface roughness.

INTRODUCTION

This study assesses the utility of reflectance spectroscopy as a tool for rapid, nondestructive analysis of deep-sea sediments. A tool such as this offers great potential for cost-effective analysis of long time series of lithologic change at high temporal resolution. Previous attempts to measure lithology from reflectance in ODP cores considered only gray-scale optical density, as recorded in black-and-white photographs (Busch, 1991). Initial success of that study motivated us to measure reflectance in an array of wavelengths as a way of isolating lithologic components. Balsam and Deaton (1991) and Balsam (1992) showed that reflectance spectra in the near-ultraviolet (nUV), visible (VIS), and near-infrared (nIR) bands, measured on discrete samples that have been carefully dried, ground, and mounted, can be calibrated to yield quantitative estimates of some aspects of lithology in deep-sea sediments.

Our contribution (Mix et al., 1992) was the development of a reflectance spectrometer system that automatically scans split core sections rapidly at closely spaced intervals. Clark et al. (1990) showed that spectrometers having high spectral resolution (on the order of 1 nm) are best suited for reliable recognition of minerals, which guided our design of an instrument suitable for use on deep-sea sediments. The Oregon State University (OSU) instrument used during Leg 138 measured reflectance spectra in 511 data channels that cover most of the VIS (455–700 nm) and nIR (700–945 nm) bands at high spectral resolution (bandwidth, 0.96 nm) fast enough (about 10 s per sample) to keep up with ODP coring operations. The instrument automatically analyzed reflectance spectra every few centimeters in more than 5 km of sedimentary sections recovered with the advanced piston corer (APC) and extended core barrel (XCB) devices in the eastern tropical Pacific Ocean. Based on shipboard results, we found that this tool helped to constrain the development of composite depth sections as cores were collected (Hagelberg et al., 1992) and yielded qualitative insight into sediment composition (Mix et al., 1992).

Here, we calibrate the reflectance data from the OSU reflectance spectrometer to yield quantitative estimates of lithology. We show that even when analyzing unprepared core surfaces, one can estimate some lithologic components with sufficient precision to yield useful quantitative geologic reconstructions. This study is preliminary. It points the way to further development of the surface scanning reflectance spectrometer and data analysis techniques to optimize the recovery of high-resolution lithologic information from this rapid remote sensing strategy.

One might ask why bother with reflectance? Wet bulk density was measured in the same samples by GRAPE (gamma ray attenuation porosity evaluator; Boyce, 1976), and this is often considered a good proxy for $CaCO_3$ contents in pelagic sediments (Mayer, 1991; Hagelberg et al., this volume). The transformation of GRAPE density into percentages of $CaCO_3$, however, depends on constancy of the wet-bulk density of the sediments diluting the calcium carbonate, as well as the grain size of the carbonate and noncarbonate components, porosity rebound, and compaction (Mayer, 1991). Where the sediment is a simple binary mixture of biogenic opal and biogenic carbonate, GRAPE is an excellent proxy for calcium carbonate contents. Where a third sedimentary component of different density and porosity (such as clay or other nonbiogenic material) is present, the GRAPE-to-calcite transform is less certain (Herbert and Mayer, 1991). This is the case in the eastern transect sites of Leg 138 (Sites 844–847). Thus, we concentrated our analysis on these eastern sites (Fig. 1), where our primary goal was to improve estimates of $CaCO_3$ percentages.

Reflectance spectroscopy is an independent approach having different assumptions, strengths, and weaknesses than GRAPE. In some cases, reflectance may be a better tool, such as for XCB cores, in which the sediments break into oblong "biscuits" within the core liners. These biscuits are damaging to the GRAPE method, because water-saturated slurry often fills the spaces between biscuits along the core edges, and GRAPE measurements integrate a finite slice across the complete core cross section. Reflectance spectroscopy is less sensitive to this problem, because sediment biscuits tend to meet along the axis of a core tube, where the reflectance is measured. A possible weakness of the reflectance method is its potential sensitivity to surface roughness and moisture content of unprepared surfaces. Thus, a second goal was to evaluate the severity of these problems for both GRAPE and reflectance methods in typical deep-sea sediments by assessing the precision of quantitative lithologic estimates, compared to ground-truth measurements. Finally, reflectance spectro-

[1] Pisias, N.G., Mayer, L.A., Janecek, T.R., Palmer-Julson, A., and van Andel, T.H. (Eds.), 1995. *Proc. ODP, Sci. Results,* 138: College Station, TX (Ocean Drilling Program).
[2] College of Oceanic and Atmospheric Sciences, Oregon State University, Corvallis, OR 97331-5503, U.S.A.
[3] Ocean Drilling Program, Texas A &M University Research Park, 1000 Discovery Drive, College Station, TX 77845-9547, U.S.A.

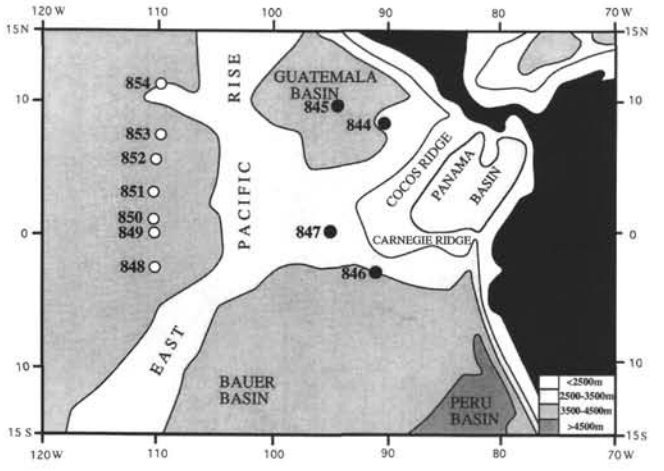

Figure 1. Leg 138 sites. Solid circles mark eastern transect sites (844–847) considered in this study.

scopy offers the potential to estimate several different lithologic parameters from the same spectral data set, should different mineral assemblages have different reflectance signatures. We consider this potential, concentrating here on the major sediment components calcium carbonate, opal, and nonbiogenic (mostly clay) sediments.

REFLECTANCE DATA

Reflectance spectra were measured at sea with a prototype instrument described in detail by Mix et al. (1992). The instrument consists of a core transport system, an illumination and sensing system, a spectrograph and detector system, and a computer control and data processing system. Similar to the ODP multisensor track, the core transport, or conveyor, moves a 1.5-m core section under the light source and detector at fixed intervals (usually 3 or 4 cm). A regulated broadband light source illuminates a spot 2-cm in diameter on a split core surface, through glass fiber-optic cables. Light is delivered and collected by a custom-designed sensing head, which hovers a fixed distance above the sediment surface. The sensing head collects directional reflectance along an axis perpendicular to the core surface. Reflected light is transferred back to the spectrograph, again through fiber-optic cables. Separation of the reflected light into its spectrum occurs in the spectrograph, which has an entrance slit, diffraction grating, focusing mirrors, and a silicon diode array detector. The computer control system consists of a 386-PC to control the mechanical system and detector, a Sun SLC UNIX workstation to receive and process the data, and a 600-Mb disk and 150-Mb tape drive to store the data.

We measured directional reflectance in 511 different wavelengths of light that ranged from about 455 to 945 nm (most of the VIS and the lower portions of the nIR bands). At each site, the standard core description included a down-core plot of three 50-nm blocks of reflectance channels (blue, red, and near-infrared), and examples of full-resolution 511-channel reflectance spectra from distinctive lithologies (Fig. 2). A preliminary look at the reflectance spectra showed that different major lithologies, such as nannofossil ooze, diatom ooze, or siliceous clay, exhibit radically different spectra (Mix et al., 1992). In addition, minor components, such as oxides, impart distinctive features to the reflectance spectra.

Some analytical noise was present in the spectra of Figure 2, especially near the low- and high-wavelength limits of the spectra. With the prototype instrument used during Leg 138, a tradeoff was made between speed of analysis and noise. To keep up with coring operations, we set short signal integration times. Typical analyses took 2.5 s. Each measurement was replicated three times, and these replicates were averaged. The total analysis time, including replicate analyses, core movement, focusing, and data storage, took about 10 s. New developments in CCD detector array technology will reduce the noise and increase the speed of analysis in the next generation of instruments. For purposes of calibrating the reflectance values to predict lithologies for this preliminary study, we smoothed the reflectance spectra by taking 20-channel block averages, starting with the longest wavelengths. This reduced the 511 channels to 25 channels, with a 19.2 nm bandwidth for use in the regression analyses.

The features we see in the Leg 138 spectra and lithologies are qualitatively consistent with features expected from laboratory experiments on pure mineral separates and known mineral mixtures (Hunt, 1977; Clark et al., 1990). For example, sediments high in calcium carbonate are visually "white" and are highly reflective in all bands measured. This is consistent with analyses of reagent calcite, which reflects close to 100% in the VIS and nIR bands (Gaffey, 1986). Nonbiogenic and biogenic calcite can differ in their reflectance character; however, in the sediments considered here, essentially all of the carbonate material is biogenic calcite.

Minor components may be important to reflectance characteristics of sediments. Oxides (commonly hematite) make the sediments appear reddish brown and are easily detected in the reflectance spectra, as shown by Deaton and Balsam (1991). Although both biogenic opal and calcite are highly reflective throughout the VIS and nIR bands measured here, they diverge in their spectra at wavelengths of less than about 500 nm (Balsam, 1992). Sulfides, such as pyrite, had relatively low reflectance throughout the bands we measured (Hunt et al., 1971b). Organic carbon is a relatively minor constituent of the sediment, but may have significant effects on reflectance (Busch, 1991) because it absorbs light in the visible bands (Hoffer, 1984; Baker and Louda, 1986), and because of its role in sedimentary redox chemistry, which controls the balance of oxides and sulfides (Lyle, 1983). The presence of water can affect the reflectance spectra and, thus, calibration of equations to predict lithology from the surface scanned data collected here must be done with samples that contain water (Clark, 1981).

GROUND-TRUTH DATA

Our calibration strategy was empirical. We sought significant relationships between "ground-truth" chemical measurements of sediment composition and accompanying reflectance spectra. For this strategy to work, the calibration data set must span the range of variation in the samples to be estimated, including the possible combinations of different lithologies. If more than one lithologic parameter is to be estimated, the various parameters must not correlate highly with each other in the calibration data set.

We calibrated reflectance spectra to predict percentages of the dominant sedimentary components, $CaCO_3$, opal, and nonbiogenic sediments using standard multiple regression techniques. The ground-truth samples analyzed chemically were taken at sea for measuring physical properties, usually one sample per 1.5-m section, from almost all cores recovered. Thus, the data set was a reasonable random sampling of a broad range of sediment types recovered from Sites 844 through 847 during Leg 138. All calibration and verification samples are from APC cores, chosen to avoid problems of lithification and disturbance in the XCB cores.

Concentrations of $CaCO_3$ (essentially all biogenic calcite) were measured at sea (Mayer, Pisias, Janecek, et al., 1992) using a Coulometrics 5011 CO_2 coulometer equipped with a System 140 carbonate carbon analyzer. A 10- to 60-mg dry sample was reacted in a solution of 2N HCl while it was heated at 65°C. The evolved CO_2 was transferred to the CO_2 coulometer cell in a helium stream. The quantity of CO_2 liberated was measured by titration in a monoethanolomine solution with a proprietary colorimetric indicator. The change in light transmittance was monitored by a photodetection cell. Reagent-grade calcite was used as a standard, and the percentage of $CaCO_3$ was

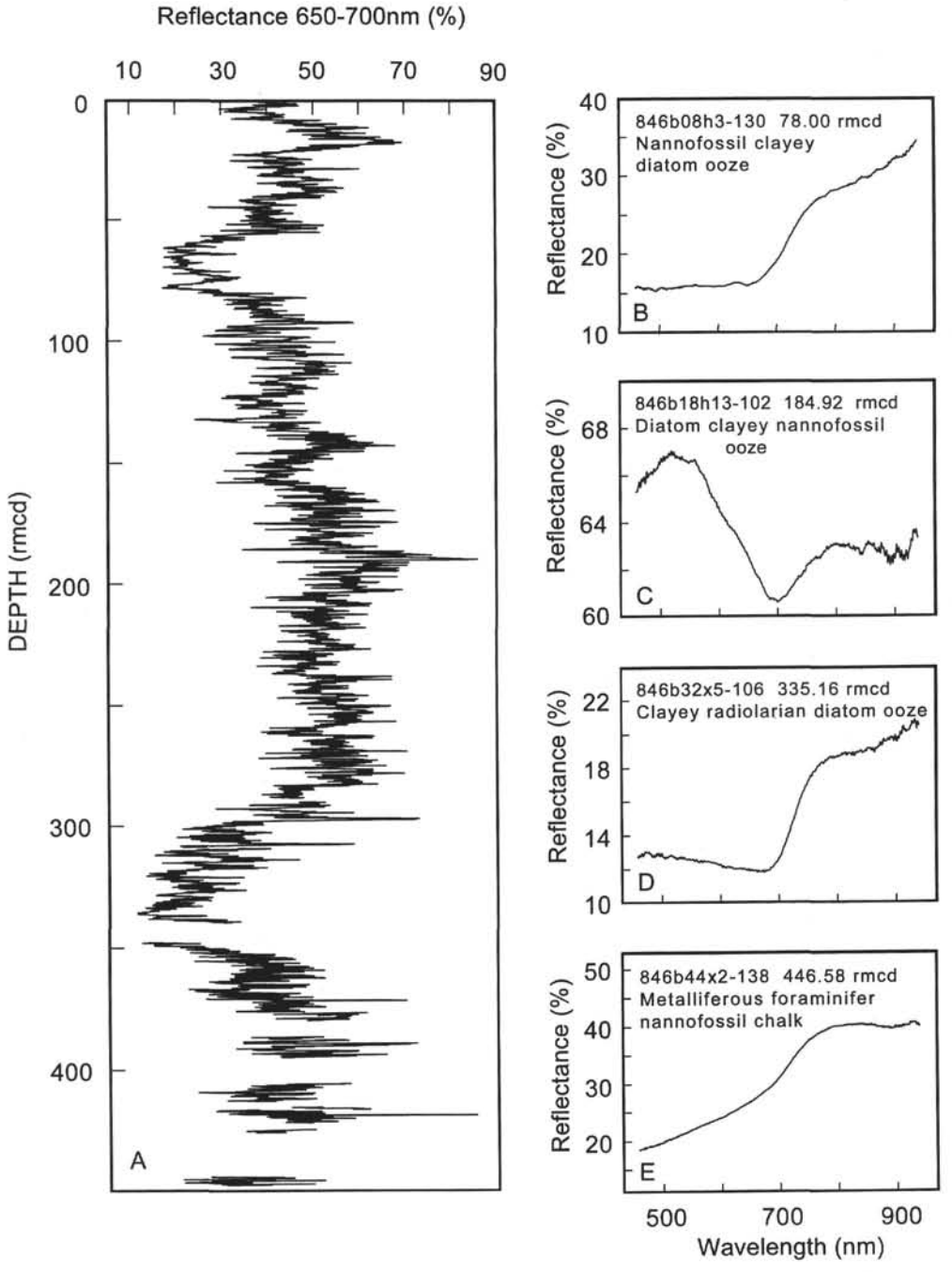

Figure 2. **A.** Percentage of reflectance in the 700- to 750-nm "red" band, in a composite section constructed by stacking and averaging analyses in Holes 846A through 846D. Depths are revised meters composite depth (rmcd), which seek to align features in all holes at the site (Hagelberg et al., this volume). **B–E.** Examples of reflectance spectra from individual samples for selected lithologies downhole. Spectra plotted are 11-channel running averages, for an effective bandwidth of ~10 nm. Note the similarity of the two diatom ooze samples (**B** and **D**) compared to the different reflectance spectra for the nannofossil ooze sample (**C**) and metalliferous chalk (**E**).

calculated from the inorganic carbon concentration (IC), assuming that all carbonate occurred as $CaCO_3$, as follows:

$$CaCO_3\% = IC\% \cdot 8.334.$$

Duplicate analyses performed during Leg 138 indicated excellent reproducibility, with an RMS error of 0.8% for $CaCO_3$ percentages.

Percentages of opal (essentially all biogenic) were determined at the Ocean Drilling Program, College Station, TX, using the wet-alkaline extraction procedure of Mortlock and Froelich (1989). A sample of 25- to 200-mg dry sediment was subjected to successive extractions with acid and peroxide to remove diluting phases (such as carbonate minerals and organic matter). Biogenic silica then was extracted for 5 hr in a 2M Na_2CO_3 solution in an 85°C water bath. The dissolved silica concentration in the extract was determined by molybdate-blue spectrometry using an absorption peak at 812 nm. Precision of this method is better than 0.1% for opal.

Nonbiogenic sediment concentration in the ground-truth samples was calculated here as:

$$\text{Nonbiogenic sediment\%} = 100 - (\text{opal\%} + \text{CaCO}_3\text{\%}).$$

Analytically, this value is not independent of the other two measurements. Although this calculation is only approximate, we think that this simple subdivision of the bulk sediment into its major components is reasonable for a first attempt at lithologic calibration. Future efforts should subdivide the nonbiogenic category into its constituents and may revise the preliminary view given here.

The three lithologic parameters span a wide range of variation in the ground-truth data set (Fig. 3). Percentages of $CaCO_3$ range from 0% to 90%. Opal concentrations range from 0% to 70%. Nonbiogenic sediment percentages range from 0% to 90%. For an ideal calibration, each of the three components should not correlate with the others. Here, the calibration and verification data sets approximate this condition for opal and nonbiogenic sediment concentrations ($r = 0.04$, $n = 398$). This is also the case for percentages of $CaCO_3$ and opal ($r = -0.25$, $n = 398$). Unfortunately, this is not the case for concentrations of $CaCO_3$ and nonbiogenic sediment. These two parameters are strongly inversely correlated ($r = -0.98$, $n = 398$). Thus, we cannot consider the equations that estimate $CaCO_3$ and nonbiogenic sediment content to be statistically independent of each other.

For purposes of developing and testing equations to estimate lithology from reflectance, the ground-truth data were divided into two groups: a calibration data set (used in the multiple regression) and a verification data set (used to check the resulting equation). To divide the data, we assembled all the analyses in order of depth within each hole and sorted odd-numbered samples into the calibration data set and even-numbered samples into the verification data set. This yielded two independent data sets of approximately 200 samples each, with similar means and distribution of variance. By showing that the precision of estimate was good in a verification data set, we gained confidence that the statistical model was not overly tuned and that the lithologic predictions were robust. The calibration and verification data sets are documented here in Tables 1 and 2. All reflectance data generated by Mix et al. (1992) have been tabulated on CD-ROM, as part of the Leg 138 shipboard data report in Mayer, Pisias, Janecek, et al. (1992).

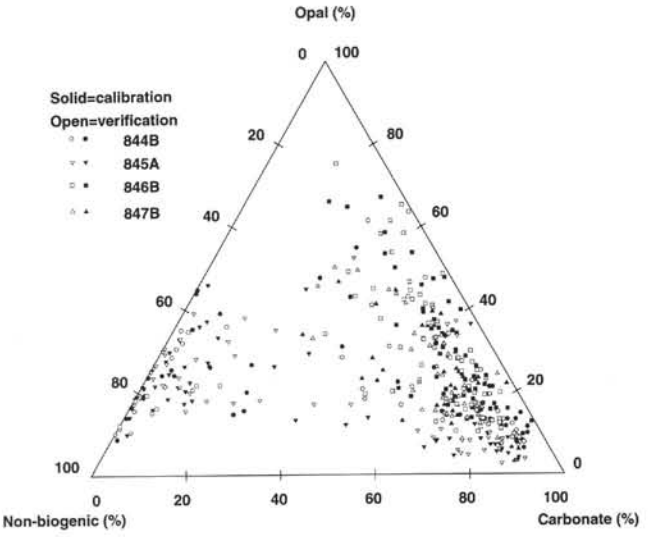

Figure 3. Ternary plot showing composition of calibration (solid symbols) and verification (open symbols) data sets. These ground-truth samples span a wide compositional range among the three end members considered here of calcium carbonate, opal, and nonbiogenic sediment.

EMPIRICAL CALIBRATIONS

Biogenic Calcium Carbonate

Figure 4 illustrates preliminary calibrations of reflectance spectra to estimate percentages of $CaCO_3$. In this multiple regression analysis, we entered terms for linear reflectance and the square of reflectance in each band to allow for weak nonlinearity. We kept only terms above a 95% confidence interval. The resulting equation for estimation of carbonate percentages is as follows:

$$\text{CaCO}_3\text{\%} = 8.42(R_{530}) - 7.14(R_{550}) - 8.37 \times 10^{-3}(R_{570})^2 + 2.94(R_{800}) - 2.21 \times 10^{-2}(R_{935})^2 - 63,$$

where R is the average reflectance within a 20-nm bandwidth centered on the subscripted wavelength. The equation has $r^2 = 0.89$, meaning that it reproduces 89% of the variance in the calibration data set. The RMS error on percentages of $CaCO_3$ estimated with this equation is ±9.3% over the full range of values from <5% to >90%. The errors in the carbonate prediction were similar in the calibration data set and the verification data set (Figs. 4A and 4B), and the verification data set has $r^2 = 0.88$. Residuals (predicted values minus measured values) were randomly distributed relative to the measured values. The estimate of $CaCO_3$ percentages from reflectance in these samples is statistically significant and appears to be unbiased and robust.

Because pure calcite is highly reflective in all bands measured here (Hunt and Salisbury, 1971; Gaffey, 1986), the reflectance calibration equation responds mostly to variations in the noncarbonate mineral assemblage that dilutes the calcite. As long as the diluent reflectance spectrum is reasonably constant within the specific wavelength bands used in the calibration equation, this strategy will work well to predict the percentage of $CaCO_3$. Of the five reflectance terms in the carbonate equation (at 95% confidence interval), two are in the nIR (800–935 nm) and three are in the middle visible bands (530–570 nm). This is not surprising. Reflectance variations in the upper visible bands are variable, because they are dominated by the relative abundance of oxides (especially hematite and goethite; Barranco et al., 1989) and clays (especially smectite; Hunt and Salisbury, 1970; Hunt et al., 1971a). In terms of reflectance spectra, the diluent of $CaCO_3$ is not constant in these bands. But outside of these bands, all of these minerals have relatively similar reflectance patterns, moderate from 800 to 950 nm and low at <550 nm. This explains why the predictive equation for calcite emphasizes the high and low ends of the spectrum, rather than the upper visible bands.

The prediction of $CaCO_3$ concentration from GRAPE density follows Mayer (1991), but uses corrections of the raw GRAPE data for porosity rebound and compaction trends optimized for each site by Mayer et al. (this volume). Once these corrections were made, the percentage of $CaCO_3$ was estimated by:

$$\text{CaCO}_3\text{\%} = -332.543\ \rho^2 + 1112.673\ \rho - 835.525,$$

where ρ is the corrected GRAPE wet bulk density. For the same samples used for the calibration and verification of reflectance spectra, GRAPE predicted the percentage of $CaCO_3$ with an RMS error of ±13% ($r^2 = 0.76$) to 15% ($r^2 = 0.80$) (Figs. 4C and 4D). The GRAPE estimation here was less precise than that based on reflectance spectra, probably because of the presence of a relatively large and variable nonbiogenic component.

Biogenic Opal

Initial attempts to calibrate equations that estimate percentages of biogenic opal ($SiO_2 \cdot nH_2O$) revealed that the reflectance spectra were sensitive to opal at low concentrations, but that calibration is less reliable at high concentrations of opal. To emphasize the lower concentrations more in the calibration equation, we performed the regression analysis after taking the log of opal concentration. As with the equation to estimate $CaCO_3$ concentration, we allowed terms for

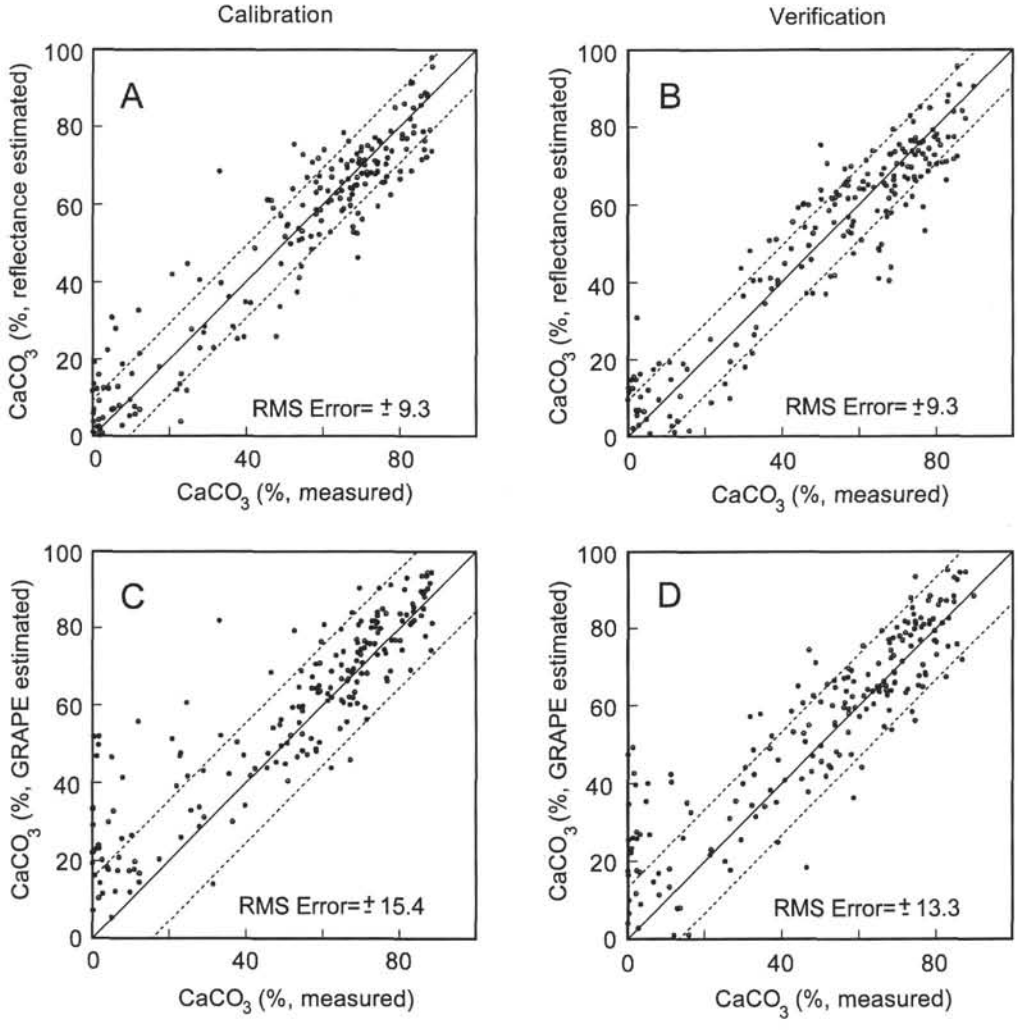

Figure 4. Estimated vs. measured percentages of $CaCO_3$. **A.** Values estimated from reflectance, calibration data set (200 samples). **B.** Values estimated from reflectance, verification data set (198 samples). **C.** Values estimated from GRAPE density, calibration data set. **D.** Values estimated from GRAPE density, verification data set.

linear reflectance and the square of reflectance into the regression equation and kept only terms above 95% confidence. The resulting equation for predicting opal concentration is

$$\log(\text{opal}\%) = 1.41 \times 10^{-3}(R_{550})^2 - 1.82 \times 10^{-3}(R_{570})^2 + 9.86 \times 10^{-3}(R_{705}) + 2.10 \times 10^{-4}(R_{935})^2 + 1.25,$$

where R is the average reflectance within a 20 nm bandwidth centered on the subscripted wavelength. After conversion to linear form, RMS errors for prediction of opal are ±9.7% ($r^2 = 0.44$) for the calibration data set and ±9.8% ($r^2 = 0.52$) for the verification data sets, respectively (Fig. 5). Although the percentage of variance in opal concentration accounted for by this equation (44%–52%) is much lower than that of $CaCO_3$, the estimates are significant at the 0.99 level ($r^2 > r^2_{(\text{critical})}$, 0.21 for $n = 200$).

Of the four terms in this equation, two are in the middle visible bands (550–570 nm), one is in the transition from red to nIR (705 nm) and one is in the near infrared (935 nm). In these bands, reflectance of reagent opal is similar to that of calcite (Balsam, 1992). The regression equation thus is responding to the difference between the relatively high reflectance of opal vs. the combined spectral character of highly reflective carbonate and the less-reflective nonbiogenic sediments. This is not ideal, but would work as long as the other mineral associations remain constant.

The reflectance equation underestimates opal percentages at measured concentrations >30%, but the precision is reasonably good (RMS error <6%) for opal concentrations less than 40%. Within the calibration data set, few samples with opal >40% have nonbiogenic sediment >30%. Thus, anomalously low estimates of opal percentages at high concentrations suggest difficulties in separating opal from carbonate with the wavelengths measured here. Balsam (1992) noted that the spectra of pure calcite and opal diverge at wavelengths less than 500 nm. Future refinements to the instrument that allow measurement of reflectance at lower visible and upper ultraviolet bands may improve the estimates of opal concentration. The present opal estimates, based on reflectance, do not capture the real amplitude of variability in the opal signal.

Nonbiogenic Sediments

Many common nonbiogenic sedimentary components are less reflective than either biogenic opal or calcium carbonate. Therefore, estimates of the concentration of nonbiogenic sediments from reflectance may be practical. Knowing the nonbiogenic component of sediments would also be useful for refining interpretation of GRAPE density data, for checking the estimates of the biogenic components, and for constraining causes of percentage variations in major lithologic components that may be diluted by nonbiogenic sediment sources.

Table 1. Calibration data set.

Core, section, interval (cm)	Depth (mbsf)	Depth (mcd)	Depth (rmcd)	$CaCO_3$ (% measured)	$CaCO_3$ (% estimated from GRAPE density)	$CaCO_3$ (% estimated from reflectance)	Opal (% measured)	Opal (% estimated from reflectance)	Nonbiogenic (% measured)	Nonbiogenic (% estimated from reflectance)
138-844B-										
1H-3, 25–27	3.26	3.26	3.26	5.60	32.81	7.31	24.10	25.94	70.29	65.85
2H-2, 46–47	6.47	7.59	7.59	4.30	29.97	–0.63	25.47	26.98	70.20	69.28
2H-4, 45–46	9.46	10.59	10.59	23.00	47.71	4.00	19.91	27.42	57.08	63.04
2H-6, 31–33	12.32	13.43	13.43	24.60	60.67	11.95	15.45	25.94	59.93	64.09
3H-2, 66–67	16.17	18.41	18.41	1.70	49.80	4.43	18.79	26.79	79.50	69.52
3H-3, 66–67	17.67	19.91	19.91	1.80	52.02	9.32	19.32	26.61	78.89	73.00
3H-5, 30–32	20.31	22.55	22.55	0.40	51.94	13.69	16.41	26.61	83.21	61.11
3H-7, 30–32	23.31	25.55	25.55	0.60	51.84	19.32	13.87	27.04	85.53	58.50
4H-3, 56–57	27.07	18.53	18.53	0.30	29.14	3.95	23.60	25.88	76.07	71.61
4H-5, 56–57	30.07	21.53	21.53	22.80	47.00	13.70	14.59	26.24	62.61	64.66
4H-7, 56–57	33.07	24.53	24.53	1.20	46.90	12.38	8.67	24.66	90.13	69.38
5H-2, 65–66	35.16	38.81	38.81	12.00	55.84	32.77	26.24	24.83	61.75	46.87
5H-4, 65–66	38.16	41.81	41.81	20.80	51.35	42.05	26.55	28.77	52.65	28.29
6H-3, 67–68	46.18	50.28	50.28	53.80	59.67	53.86	22.28	15.92	23.93	30.22
6H-5, 68–69	49.19	53.28	53.28	7.90	41.46	18.82	39.08	22.34	53.00	62.23
7H-2, 70–71	54.21	60.91	60.91	0.30	33.52	6.08	44.77	22.44	54.89	74.86
7H-4, 70–71	57.21	63.91	63.91	0.40	22.23	7.08	43.95	23.28	55.67	72.57
7H-6, 70–71	60.21	66.91	66.91	54.70	48.32	53.14	20.75	20.32	24.56	28.84
8H-1, 145–146	62.96	70.09	70.09	37.70	50.53	25.32	30.90	24.27	31.39	49.55
8H-4, 30–32	66.31	73.44	73.44	70.90	76.64	70.18	14.19	14.06	14.92	14.78
8H-6, 145–146	70.46	77.61	77.61	28.90	43.17	26.98	54.95	29.44	16.19	41.34
9H-2, 66–67	73.17	81.81	81.81	59.70	76.49	55.81	25.70	25.82	14.60	18.53
9H-4, 66–67	76.17	84.81	84.81	73.60	81.86	71.24	16.29	14.76	10.11	7.11
9H-6, 66–67	79.17	87.80	87.80	86.10	89.11	78.83	8.59	10.99	5.30	10.01
10H-1, 70–71	81.21	91.84	91.84	87.00	93.56	72.25	8.13	15.31	4.87	9.99
10H-3, 70–71	84.21	94.84	94.84	81.90	93.07	77.05	11.53	11.80	6.57	10.94
10H-5, 70–71	87.21	97.84	97.84	86.40	88.13	74.22	9.62	14.66	3.98	7.73
11H-1, 70–71	90.71	104.21	104.21	77.70	91.25	78.81	13.18	11.19	9.11	4.78
11H-3, 70–71	93.71	107.21	107.21	73.60	80.25	67.87	21.09	23.39	5.29	7.28
11H-5, 70–71	96.71	110.21	110.21	83.10	81.48	68.70	13.24	15.31	3.64	15.01
11H-7, 70–71	99.71	113.21	113.21	74.30	78.78	59.62	21.09	32.28	4.59	12.70
12H-2, 65–66	101.66	115.17	115.17	80.10	83.80	66.62	15.78	21.88	4.12	11.27
12H-5, 65–66	106.16	119.68	119.68	86.50	89.60	76.49	11.38	14.49	2.11	1.29
12H-7, 65–66	109.16	122.68	122.68	24.80	41.79	44.80	47.64	55.85	27.57	5.12
15H-2, 65–66	130.16	145.15	145.15	81.30	90.10	85.92	13.24	8.04	5.44	6.89
16H-4, 100–102	143.01	159.20	159.20	83.40	86.38	91.45	14.72	6.47	1.88	6.23
18H-6, 100–102	165.01	182.07	182.07	87.30	94.44	87.79	9.86	8.18	2.84	11.48
19H-6, 100–102	174.51	191.72	191.72	74.70	90.36	76.36	15.35	12.27	9.97	9.70
20H-6, 100–102	184.01	202.65	202.65	88.30	94.46	73.82	6.27	15.28	5.44	11.65
138-845A-										
1H-4, 145–150	5.98	5.96	5.96	3.00	–56.98	12.64	24.10	32.36	72.93	54.33
2H-1, 40–42	8.01	8.88	8.88	3.92	18.42	22.39	35.32	30.55	60.79	41.14
2H-3, 40–42	11.01	11.90	11.90	6.00	12.20	28.04	37.24	26.85	56.74	40.66
2H-5, 40–42	14.01	14.90	14.90	1.75	24.03	2.68	29.85	26.92	68.40	62.70
3H-1, 40–42	17.51	18.36	18.36	5.08	5.57	30.92	35.97	28.91	58.95	32.04
3H-3, 40–42	20.51	21.38	21.38	10.33	26.61	16.32	33.27	29.17	56.42	52.28
3H-5, 40–42	23.51	24.38	24.38	4.25	17.75	12.47	24.49	26.48	71.24	55.90
3H-7, 40–42	26.51	27.38	27.38	12.25	14.59	21.59	26.06	26.79	61.71	48.03
4H-2, 40–42	28.51	30.65	30.65	6.67	17.54	13.01	26.30	26.30	67.01	56.73
4H-4, 40–42	31.51	33.65	33.65	2.08	14.37	1.85	27.61	24.83	70.28	69.84
4H-6, 40–42	34.51	36.65	36.65	2.67	20.26	0.84	9.89	25.47	87.44	69.11
5H-1, 100–102	37.11	40.63	40.63	1.17	23.07	2.57	14.03	25.47	84.79	58.25
5H-3, 100–102	40.11	43.63	43.63	5.08	46.65	7.00	15.92	26.36	79.01	60.82
5H-6, 102–104	44.63	48.13	48.13	11.17	19.83	5.88	27.23	26.36	61.60	60.91
6H-3, 30–32	48.91	52.98	52.98	1.75	10.50	16.06	29.79	27.54	68.43	55.96
7H-3, 99–101	59.10	63.94	63.94	0.08	22.15	11.81	18.62	25.64	81.32	61.78
10H-1, 100–102	84.61	93.10	93.10	9.83	12.03	9.64	20.32	24.27	69.84	69.13
10H-3, 103–105	87.64	96.10	96.10	7.00	20.95	8.12	18.45	23.66	74.54	70.17
10H-5, 101–103	90.62	99.10	99.10	11.00	17.86	7.86	17.34	23.44	71.66	69.71
11H-1, 100–102	94.11	103.88	103.88	2.75	11.61	4.87	21.58	23.88	75.69	68.09
11H-4, 100–102	98.61	108.38	108.38	9.67	17.52	5.49	22.49	24.10	67.86	66.56
11H-6, 100–102	101.61	111.38	111.38	1.88	23.28	0.39	46.03	22.75	52.05	67.43
12H-2, 100–102	105.11	116.45	116.45	23.17	26.00	16.24	44.98	26.00	31.88	55.35
12H-4, 100–102	108.11	119.42	119.42	31.50	14.08	23.03	29.31	26.18	39.19	49.69
12H-6, 100–102	111.11	122.45	122.45	7.75	25.75	2.98	21.33	23.66	70.93	64.06
13H-2, 100–102	114.61	127.23	127.23	12.33	16.84	7.06	18.07	22.44	69.62	67.22
13H-5, 100–102	119.11	131.73	131.73	0.25	7.34	–1.67	26.67	22.28	73.09	73.89
14H-2, 100–102	124.11	138.08	138.08	0.17	19.42	–2.12	19.05	20.56	80.79	79.64
14H-4, 100–102	127.11	141.10	141.10	0.67	16.30	–2.78	21.09	21.23	78.22	76.68
14H-6, 100–102	130.11	144.10	144.10	0.25	33.27	1.20	25.41	20.70	74.35	78.10
15H-2, 108–110	133.69	149.56	149.56	0.17	–3.17	–6.69	21.43	20.65	78.41	81.14
15H-5, 108–110	138.19	154.06	154.06	25.75	32.96	27.81	26.18	27.61	48.10	38.62
16H-1, 110–112	141.71	159.44	159.44	36.59	30.11	28.54	13.24	36.73	50.15	47.38
16H-3, 110–112	144.71	162.43	162.43	47.84	45.43	25.99	12.05	33.65	40.12	46.97
16H-5, 110–112	147.71	165.43	165.43	51.67	52.26	49.93	13.80	19.32	34.53	32.91
17H-1, 101–103	151.12	169.93	169.93	68.84	71.57	65.01	8.02	8.73	23.14	30.66
17H-3, 101–103	154.12	172.93	172.93	74.34	73.12	70.85	4.52	5.74	21.14	25.46
17H-5, 101–103	157.12	175.93	175.93	71.42	56.32	68.35	8.57	8.32	20.01	31.34
18H-1, 100–102	160.61	179.87	179.87	68.92	66.10	66.94	8.30	8.65	22.78	26.91
18H-4, 100–102	165.11	184.40	184.40	67.09	60.21	64.33	6.56	10.74	26.35	25.75
18H-6, 100–102	168.11	187.40	187.40	80.76	74.38	78.11	7.14	8.34	12.10	14.38
19H-2, 100–102	171.61	192.28	192.28	88.26	74.30	97.91	4.08	4.27	7.66	–0.44
19H-4, 99–101	174.60	195.24	195.24	88.42	81.29	95.55	3.40	5.51	8.18	1.70
19H-6, 100–102	177.61	198.28	198.28	82.92	69.22	91.29	5.45	7.64	11.64	1.10
20H-2, 99–101	181.10	203.41	203.41	75.01	79.86	76.03	12.05	10.00	12.95	12.94
20H-4, 101–103	184.12	206.46	206.46	82.76	81.11	82.12	7.21	9.84	10.03	9.62

Table 1 (continued).

Core, section, interval (cm)	Depth (mbsf)	Depth (mcd)	Depth (rmcd)	$CaCO_3$ (% measured)	$CaCO_3$ (% estimated from GRAPE density)	$CaCO_3$ (% estimated from reflectance)	Opal (% measured)	Opal (% estimated from reflectance)	Nonbiogenic (% measured)	Nonbiogenic (% estimated from reflectance)
20H-6, 102–104	187.13	209.45	209.45	81.76	83.49	74.34	7.14	11.07	11.10	17.01
21H-2, 100–102	190.61	213.85	213.85	78.84	76.89	84.93	9.79	9.75	11.37	5.67
21H-4, 100–102	193.61	216.85	216.85	78.01	76.82	73.74	8.57	13.03	13.42	16.11
21H-6, 100–102	196.61	219.85	219.85	85.59	83.33	87.90	5.00	8.18	9.41	3.35
22H-2, 101–103	200.12	225.35	225.35	83.67	85.50	78.48	6.10	10.33	10.24	15.43
22H-4, 100–102	203.11	228.35	228.35	83.76	82.02	80.25	5.68	11.25	10.56	7.73
22H-6, 100–102	206.11	231.35	231.35	83.59	84.32	84.91	8.81	10.91	7.60	0.89
138-846B-										
1H-4, 101–103	5.52	5.58	5.63	58.25	48.77	58.68	33.34	31.70	8.40	10.05
2H-1, 108–110	8.09	8.84	8.94	62.17	43.91	61.09	36.31	31.77	1.55	11.43
2H-3, 97–99	10.98	11.61	11.64	68.34	63.45	64.88	26.06	25.00	5.58	6.58
2H-5, 103–105	14.04	14.63	14.64	77.67	68.87	62.47	15.78	31.84	6.55	7.10
2H-7, 51–53	16.52	17.14	17.16	80.17	76.84	68.64	12.68	15.67	7.15	13.29
3H-2, 104–106	19.05	21.33	21.55	69.17	73.74	57.77	23.55	31.33	7.30	11.49
3H-4, 104–106	22.05	24.11	24.11	64.92	66.88	58.41	28.51	29.24	6.59	10.08
4H-2, 103–105	28.54	31.67	31.67	50.75	50.29	54.44	39.17	35.16	10.05	10.76
4H-4, 103–105	31.54	34.63	34.60	53.84	64.77	50.81	20.09	35.48	26.07	17.90
4H-6, 118–120	34.69	37.85	37.88	71.59	68.33	67.66	23.71	25.47	4.68	7.63
5H-2, 104–106	38.05	43.28	43.30	62.09	64.59	52.96	29.99	30.62	7.92	12.37
5H-4, 104–106	41.05	46.12	45.97	57.17	64.51	48.48	31.62	31.41	11.18	21.69
5H-6, 104–106	44.05	49.76	50.20	69.01	60.53	52.59	25.12	33.81	5.90	14.93
6H-2, 104–106	47.55	54.06	54.06	50.25	44.94	51.78	39.99	30.76	9.73	16.25
6H-4, 104–106	50.55	57.06	57.06	35.59	42.39	36.24	53.58	30.48	10.89	32.65
6H-6, 102–104	53.53	60.02	60.02	39.42	47.12	25.82	50.12	38.99	10.50	27.28
7H-2, 104–106	57.05	65.35	65.34	17.50	20.46	18.11	66.22	30.13	16.34	47.36
7H-6, 108–110	63.09	71.67	71.94	27.92	28.79	22.95	67.14	39.54	4.93	29.74
8H-1, 38–40	64.39	74.01	73.95	41.17	41.89	34.62	53.70	35.56	5.08	19.67
8H-3, 103–105	68.04	77.72	77.72	22.00	39.24	12.22	64.86	34.99	13.16	34.05
8H-5, 103–105	71.04	80.63	80.57	53.92	55.55	41.14	37.33	40.55	8.71	13.50
9H-2, 104–106	76.05	85.86	85.50	54.50	69.01	44.09	35.16	34.43	10.31	19.06
9H-4, 104–106	79.05	89.20	89.19	71.01	59.49	65.25	20.42	28.25	8.59	11.50
9H-6, 104–106	82.05	92.47	92.65	76.67	67.08	67.20	16.98	22.39	6.33	1.72
10H-2, 114–116	85.65	98.21	98.22	59.13	65.15	67.32	34.75	27.42	6.12	6.62
10H-4, 113–115	88.64	101.23	101.32	48.84	55.00	33.78	47.32	51.52	3.80	9.17
10H-6, 103–105	91.54	104.23	104.41	46.59	68.61	61.06	36.06	28.84	17.34	12.14
11H-2, 103–105	95.04	108.84	109.05	67.67	68.52	64.06	22.75	23.28	9.58	10.69
11H-4, 100–102	98.01	111.56	111.62	33.04	81.94	68.55	58.61	18.32	8.34	7.06
11H-6, 102–104	101.03	114.81	115.03	51.00	40.56	54.91	47.64	45.29	1.37	7.11
12H-4, 103–105	107.54	122.38	122.43	33.50	52.20	39.81	42.95	32.06	23.52	28.15
12H-6, 100–102	110.51	125.74	126.11	58.25	64.46	63.15	33.50	29.11	8.23	7.69
13H-2, 103–105	114.04	130.30	130.15	47.09	54.20	59.10	45.81	31.92	7.04	5.73
13H-4, 102–104	117.03	133.65	133.95	55.92	47.30	67.00	35.32	29.24	8.75	9.98
13H-6, 102–104	120.03	136.98	137.40	63.51	72.95	63.01	27.86	34.12	8.61	9.16
14H-2, 102–104	123.53	140.70	140.76	73.59	75.96	77.19	13.58	12.62	12.84	7.25
14H-4, 102–104	126.53	143.76	143.83	72.59	80.12	68.22	15.96	23.44	11.46	9.50
14H-6, 103–105	129.54	146.75	146.82	76.51	83.77	74.43	13.34	18.32	10.16	2.01
15H-3, 102–104	134.53	154.21	154.20	59.30	70.96	64.29	28.97	23.60	11.73	10.47
15H-5, 94–96	137.45	157.32	157.48	57.34	67.42	70.88	33.96	20.84	8.73	13.22
16H-1, 104–106	141.05	160.68	160.22	66.59	69.09	66.59	15.14	24.66	18.28	9.33
16H-3, 102–104	144.03	164.24	164.25	58.25	70.73	65.79	18.79	20.46	22.95	13.34
16H-6, 102–104	148.53	168.57	168.48	64.76	79.69	71.40	20.42	19.19	14.84	3.21
17H-2, 102–104	152.03	173.25	173.22	64.84	61.36	63.59	19.32	30.97	15.85	4.52
17H-4, 102–104	155.03	176.25	176.23	60.34	80.88	74.12	34.04	18.66	5.63	5.71
17H-6, 102–104	158.03	179.14	178.99	69.26	80.82	70.67	18.97	22.70	11.77	9.94
18H-2, 103–105	161.54	183.35	183.33	61.34	63.05	60.58	23.39	33.96	15.27	2.73
18H-4, 103–105	164.54	186.36	186.35	74.26	83.17	68.33	17.06	25.06	8.67	10.78
18H-6, 102–104	167.53	189.39	189.40	85.76	93.60	71.63	8.09	6.07	6.15	32.40
19H-2, 103–105	171.04	194.82	194.82	72.76	81.84	74.24	13.24	16.94	14.01	4.39
19H-4, 103–105	174.04	197.82	197.82	69.92	81.79	70.43	20.04	22.03	10.02	4.73
19H-6, 103–105	177.04	200.73	200.64	74.26	84.11	68.53	19.23	25.06	6.50	7.40
20H-3, 103–105	182.04	207.62	207.61	71.67	76.17	75.14	18.07	16.44	10.28	8.61
20H-5, 103–105	185.04	211.23	211.46	67.59	83.98	71.24	18.62	22.03	13.81	5.31
21H-1, 103–105	188.54	215.50	215.51	74.17	81.52	70.40	15.14	21.53	10.70	8.52
21H-3, 103–105	191.54	218.47	218.47	72.34	75.97	68.15	21.63	27.29	6.04	5.36
21H-5, 103–105	194.54	221.47	221.47	75.59	84.94	65.72	13.49	29.65	10.91	–2.85
22H-1, 103–105	198.04	228.47	228.46	69.51	90.39	71.70	20.37	18.79	10.12	4.70
22H-3, 103–105	201.04	231.47	231.47	66.26	55.80	70.29	24.15	24.49	9.60	–2.09
22H-5, 103–105	204.04	234.46	234.45	54.84	59.86	72.86	41.69	19.63	3.44	5.44
138-847B-										
1H-1, 124–126	1.25	1.28	1.30	67.09	45.96	59.73	16.67	21.09	16.25	14.08
1H-3, 103–105	4.04	4.02	4.02	58.34	48.22	57.50	39.81	24.04	1.88	16.68
1H-5, 19–21	6.20	6.32	6.48	59.17	50.46	52.29	30.62	20.28	10.23	19.29
2H-2, 102–104	9.03	9.16	9.17	67.59	68.55	62.61	17.62	22.65	14.80	11.65
2H-4, 102–104	12.03	12.15	12.15	76.51	73.50	70.39	15.63	12.22	7.85	14.33
2H-6, 101–103	15.02	15.07	14.99	86.67	77.94	88.80	12.74	7.45	0.58	–0.68
3H-2, 102–104	18.53	18.94	19.01	65.42	60.77	58.94	21.28	16.11	13.30	19.63
3H-4, 31–33	20.82	21.12	21.09	45.71	47.65	61.22	23.23	21.09	31.07	13.51
3H-6, 102–104	24.53	24.83	24.80	69.92	73.21	73.78	22.70	13.15	7.37	7.09
4H-1, 102–104	26.53	29.35	29.35	76.84	66.29	71.99	21.93	14.79	1.23	10.07
4H-3, 102–104	29.53	32.43	32.48	49.17	56.31	57.10	22.70	23.55	28.12	15.50
4H-5, 102–104	32.53	35.45	35.56	49.17	49.58	44.78	25.18	19.28	25.67	30.66
4H-7, 32–34	34.83	37.77	37.84	64.51	53.99	61.60	25.41	17.18	10.06	16.60
5H-2, 103–105	37.54	40.32	40.32	66.92	62.20	61.38	23.44	21.93	9.65	13.76
5H-4, 103–105	40.54	43.38	43.46	62.34	62.11	69.15	29.38	19.63	8.28	7.35
5H-6, 108–110	43.59	46.34	46.27	57.00	51.49	51.87	31.77	26.79	11.24	18.86
6H-1, 102–104	45.53	50.62	50.64	39.84	34.23	34.90	41.21	26.42	18.99	29.74

Table 1 (continued).

Core, section, interval (cm)	Depth (mbsf)	Depth (mcd)	Depth (rmcd)	$CaCO_3$ (% measured)	$CaCO_3$ (% estimated from GRAPE density)	$CaCO_3$ (% estimated from reflectance)	Opal (% measured)	Opal (% estimated from reflectance)	Nonbiogenic (% measured)	Nonbiogenic (% estimated from reflectance)
6H-3, 102–104	48.53	53.47	53.33	53.34	46.70	37.52	35.81	25.06	10.82	32.48
6H-5, 103–105	51.54	56.70	56.78	59.34	63.73	58.60	12.94	22.96	27.71	13.88
6H-7, 27–29	53.78	59.01	59.17	29.17	31.22	28.50	46.67	37.33	24.15	28.95
7H-2, 103–105	56.54	63.15	63.03	27.92	33.81	40.66	33.88	26.30	38.22	30.12
7H-4, 102–104	59.53	66.12	65.99	45.50	43.91	61.21	28.12	23.23	26.38	11.50
7H-6, 103–105	62.54	69.04	68.72	42.30	43.80	48.73	44.57	29.58	13.13	11.49
8H-3, 102–104	67.53	75.92	76.06	64.84	70.52	65.85	16.52	18.75	18.64	9.10
8H-5, 100–102	70.51	78.84	78.96	61.34	61.25	63.49	28.31	26.06	10.37	6.10
9H-1, 103–105	74.04	83.38	83.22	66.67	66.84	76.25	20.61	15.24	12.73	4.18
9H-3, 102–104	77.03	86.38	86.25	54.67	52.64	51.21	35.89	28.84	9.46	16.36
9H-5, 104–106	80.05	89.47	89.42	80.67	81.97	77.11	11.94	13.21	7.40	3.51
9H-7, 33–35	82.34	91.72	91.62	52.59	79.33	75.50	39.36	10.50	8.04	11.85
10H-3, 104–106	86.55	96.80	96.81	70.92	74.90	71.42	21.78	20.23	7.29	3.13
10H-5, 23–25	88.74	98.95	98.95	70.17	68.25	68.00	23.33	15.14	6.51	14.08
10H-7, 43–45	91.94	102.15	102.15	54.75	58.59	59.83	38.73	21.63	6.56	11.33
11H-2, 33–35	93.84	106.60	106.40	66.34	66.32	69.51	16.67	17.30	17.00	5.15
11H-4, 33–35	96.84	109.70	109.66	69.17	76.18	46.28	16.56	22.75	14.27	22.69
11H-6, 33–35	99.84	112.68	112.63	70.09	74.60	74.78	12.08	15.14	17.84	2.14
12H-2, 33–35	103.34	116.39	116.41	86.17	85.05	78.78	7.62	10.40	6.21	3.28
12H-4, 33–35	106.34	119.44	119.50	68.01	69.54	52.92	14.13	16.07	17.85	28.07
12H-6, 33–35	109.34	122.35	122.33	76.17	74.38	65.81	13.00	13.55	10.84	18.35
13H-1, 82–84	111.83	125.97	126.09	67.90	62.03	54.25	18.49	17.46	13.60	20.70
13H-3, 41–43	114.42	128.41	128.40	70.34	71.04	56.21	14.13	14.59	15.55	26.23
13H-5, 33–35	117.34	131.36	131.39	85.59	89.58	85.57	6.38	6.97	8.02	4.37
13H-7, 33–35	120.34	134.40	134.46	87.88	91.71	79.23	3.06	8.85	9.06	6.81
14H-2, 33–35	122.34	137.88	137.97	87.26	90.30	88.35	5.98	6.03	6.76	0.36
14H-4, 102–104	126.03	141.52	141.53	68.84	77.02	73.06	15.14	13.96	16.03	10.35
14H-6, 102–104	129.03	144.54	144.59	65.42	73.93	78.43	24.60	16.67	10.00	2.54
15H-1, 64–66	130.65	145.75	145.47	52.17	59.49	64.03	35.89	22.13	11.93	9.35
15H-3, 33–35	133.34	146.65	145.78	62.34	68.86	67.08	24.60	23.12	13.08	6.91
15H-6, 33–35	137.84	148.16	146.28	58.84	63.24	71.83	31.41	17.95	9.74	7.54

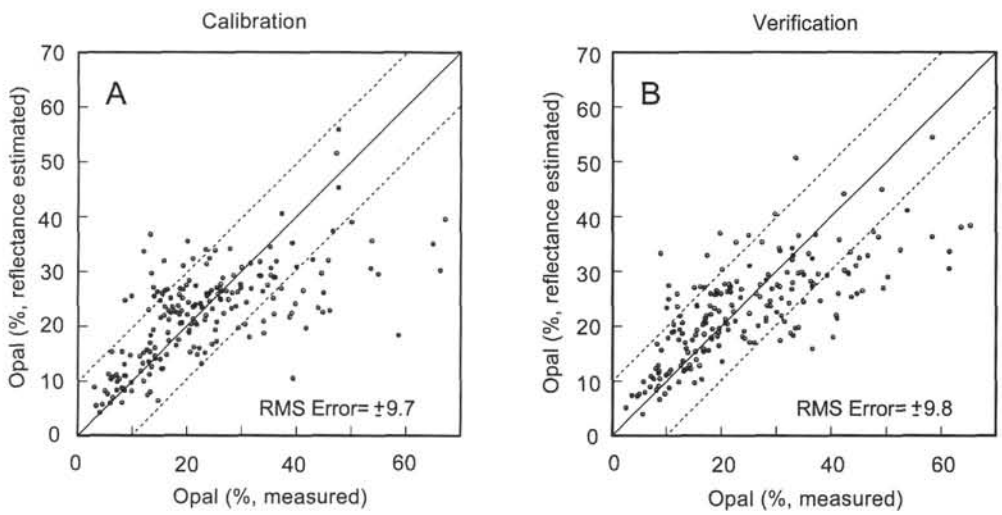

Figure 5. Estimated vs. measured percentages of biogenic opal. **A.** Values estimated from reflectance, calibration data set. **B.** Values estimated from reflectance, verification data set. The reflectance equation tends to underestimate opal percentages at higher concentrations.

Nonbiogenic material can include various components, such as clay minerals, oxides, sulfides, and sulfates, and with our simplistic method of calculation also includes traces of organic matter. We proceeded because the nonbiogenic sediments in this area are relatively simple, composed almost entirely of smectite clay (Heath et al., 1974; Schumann and Nagel, 1982; Zimmerman, 1982), although minor or trace quantities of barite, kaolinite, illite, quartz, and zeolites may be present.

Calibration of estimates for nonbiogenic sediment is shown in Figure 6. The nonbiogenic component ranges from 0% to 90% in the calibration data set. The regression equation again allows for linear and squared terms of reflectance and keeps only the terms above the 95% confidence interval. Concentration of total nonbiogenic sediments can be estimated with

$$\text{Nonbiogenic\%} = -3.94(R_{470}) + 1.83 \times 10^{2}(R_{470})^2 + 22.6(R_{665}) - 2.44 \times 10^{-1}(R_{685})^2 - 25.2(R_{705}) + 4.83 \times 10^{-2}(R_{705})^2 + 1.51(R_{935}) + 138.8,$$

where R is the average reflectance within a 20-nm bandwidth centered on the subscripted wavelength. RMS error on predictions of nonbiogenic sediment is ±10.2% ($r^2 = 0.84$) for the calibration data set, and ±10.4% ($r^2 = 0.83$) for the verification data set. This indicates that the equation reproduces at least 83% of the variance in the ground-truth data set. Although the measured points are clustered at nonbiogenic concentrations of less than 20%, the scatter of estimates appears relatively constant over the full range of variation. Three of the five different wavelength bands that appear as terms in this equation do not appear in the equations to predict biogenic calcium carbonate or

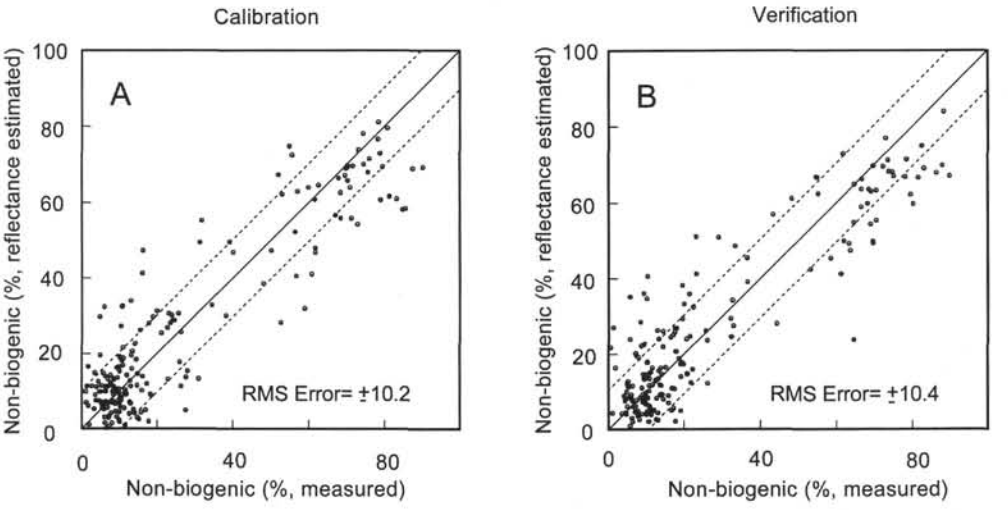

Figure 6. Estimated vs. measured percentages of nonbiogenic sediments. Measured values approximate the percentage of nonbiogenic sediment as 100 – ($CaCO_3$% + opal%) without attempting to isolate the various components contributing to the material. The major contributor to nonbiogenic sediment is smectite clay. **A.** Values estimated from reflectance, calibration data set. **B.** Values estimated from reflectance, verification data set.

biogenic opal. This suggests some independence of the estimates of nonbiogenic and biogenic components. Carbonate and nonbiogenic sediments are inversely correlated in the calibration and verification data sets, however, so we cannot confirm that these two parameters can be estimated independently of each other.

DOWNHOLE ESTIMATES

Eastern Pacific Sediment History

Here, we estimate time series of sedimentary percentages of $CaCO_3$, opal, and nonbiogenic sediment in Site 846 from the eastern transect of Leg 138, southwest of the Galapagos Archipelago. Our purpose is to evaluate the potential for multicomponent reconstructions of lithologic history from reflectance spectroscopy. The time scale we used is based on benthic foraminifer oxygen isotope stratigraphy in Holes 846B, 846C, and 846D (0–1.8 Ma by Mix et al., this volume; 1.8–3.6 Ma by Shackleton et al., this volume).

Time series of the three components estimated from reflectance are given in Figure 7. In this figure, ground-truth analyses are shown as solid dots. The two estimated components that vary most are $CaCO_3$ and nonbiogenic sediments, and these are strongly negatively correlated ($r = -0.95$), as they were in the calibration and verification data sets. The estimates of $CaCO_3$ appear reasonable throughout the past 3.6 Ma (Fig. 7A).

Estimated opal is less variable than the other components. This low amplitude is partially an artifact of the failure of the regression equation to estimate high opal concentrations. This is shown in Figure 7B, where discrete opal measurements (filled circles) often are higher than downhole opal estimated from reflectance spectra.

The estimates of nonbiogenic sediment percentages are somewhat more reliable that those of opal, but at times they overestimate the true concentration of nonbiogenic sediments, such as in the interval between 1.5 and 2.1 Ma (Fig. 7B). The intervals of major disagreement between reflectance estimates and ground-truth measurements of nonbiogenic sediments may indicate the presence of a nonbiogenic lithologic component that is not well represented in the calibration data set. Our partially successful attempt to predict nonbiogenic sediment composition downhole focuses our attention on areas where more study will be needed to define the lithologic character. Our estimate of nonbiogenic sediment concentration in the ground-truth data set was simplistic and, clearly, can be improved.

We conclude that the estimates of $CaCO_3$ percentage from reflectance spectroscopy are useable for studying geologic history in these sites, that the estimates of nonbiogenic sediment are useful but require additional study to better characterize its many components, and that estimates of opal are not yet reliable in all situations.

Comparing GRAPE with Reflectance Estimates of $CaCO_3$ Percentages

In Figure 8, we compare downhole estimates of $CaCO_3$ based on reflectance and GRAPE density for typical 50-m intervals of APC and XCB cores from Site 846. In APC cores (Fig. 8A), clearly, both estimates are sensing the same carbonate variations, although in detail the records sometimes diverge. Estimation of $CaCO_3$ percentages by both GRAPE and reflectance correspond reasonably well to downhole discrete carbonate measurements (denoted by filled circles).

GRAPE measurements may be influenced strongly by drilling disturbance, such as injection of water (common in the upper portion of Section 1 in many APC cores), or the tendency of sediments recovered by XCB to break into "biscuits" surrounded by soupy disturbed sediments near the core edges. Because GRAPE measurements integrate the complete cross section of the core, they cannot avoid the disturbed intervals, which appear as anomalously low density (and thus low inferred $CaCO_3$) values. This biscuit effect is shown in estimates of downhole carbonate percentage for XCB cores from depths of 280 to 330 rmcd in Hole 846B (Fig. 8B). Here, the GRAPE estimates of $CaCO_3$ exhibit occasional spikes of anomalously low percentage. Reflectance is less sensitive to the biscuit effect in the XCB sections, because sediment biscuits tend to meet with minimal gaps between them where reflectance is measured, along the axis of the core. We conclude that reflectance estimates are less sensitive to errors associated with sediment disturbance and biscuit formation induced by XCB coring in partially lithified sediments.

However, reflectance may be sensitive to other errors in XCB cores. For example, XCB cores are sometimes difficult to split, and surface roughness associated with imperfect splitting may induce errors in our measurements of reflectance spectra. We tested for this effect by estimating $CaCO_3$ percentage by GRAPE and by reflectance for 107 samples from XCB cores that have chemical ground-truth measurements at the same location as both GRAPE and reflectance measurements (Table 3). In these samples, which were carefully

Table 2. Verification data set.

Core, section, interval (cm)	Depth (mbsf)	Depth (mcd)	Depth (rmcd)	$CaCO_3$ (% measured)	$CaCO_3$ (% estimated from GRAPE density)	$CaCO_3$ (% estimated from reflectance)	Opal (% measured)	Opal (% estimated from reflectance)	Nonbiogenic (% measured)	Nonbiogenic (% estimated from reflectance)
138-844B-										
2H-1, 31–33	4.82	5.93	5.93	4.90	35.42	4.65	21.49	26.87	73.61	71.22
2H-3, 27–29	7.78	8.89	8.89	16.50	32.64	–4.88	21.66	26.20	61.84	72.85
2H-5, 45–46	10.96	12.09	12.09	11.50	40.35	2.84	21.69	27.21	66.81	66.32
2H-7, 25–26	13.76	14.89	14.89	5.80	26.89	0.98	16.12	27.12	78.08	66.87
3H-3, 30–32	17.31	19.55	19.55	0.10	47.44	9.77	11.97	25.86	87.93	69.85
3H-4, 36–38	18.87	21.13	21.13	5.40	40.06	12.17	15.06	26.96	79.54	62.21
3H-6, 30–32	21.81	24.05	24.05	0.40	34.77	11.73	18.05	25.90	81.55	66.67
4H-2, 56–57	25.57	17.03	17.03	11.20	42.32	14.90	20.57	27.63	68.23	59.85
4H-4, 56–57	28.57	20.03	20.03	2.20	39.70	7.03	19.31	25.95	78.49	71.44
4H-6, 56–57	31.57	23.03	23.03	1.40	49.29	12.62	15.54	23.72	83.06	69.08
5H-1, 65–66	33.66	37.31	37.31	47.10	74.35	49.46	20.67	21.25	32.23	29.46
5H-3, 65–66	36.66	40.31	40.31	48.80	71.04	53.95	18.26	17.65	32.94	27.52
5H-5, 119–120	40.20	43.83	43.83	53.80	55.68	60.09	36.55	15.88	9.65	22.69
6H-2, 78–79	44.79	48.87	48.87	57.20	67.36	61.60	16.73	15.84	26.07	23.68
6H-4, 68–69	47.69	51.78	51.78	67.80	77.04	61.61	12.99	13.64	19.21	14.22
6H-6, 68–69	50.69	54.78	54.78	32.60	48.64	40.45	34.03	19.74	33.37	48.61
7H-1, 70–71	52.71	59.40	59.40	10.90	13.44	19.32	35.84	33.21	53.26	42.42
7H-5, 70–71	58.71	65.41	65.41	39.00	46.01	39.50	28.29	23.65	32.71	34.28
7H-7, 70–71	61.71	68.41	68.41	57.40	59.20	53.10	21.05	20.39	21.55	24.74
8H-5, 145–146	68.96	76.11	76.11	69.30	68.51	62.71	22.51	20.93	8.19	19.15
9H-1, 66–67	71.67	80.32	80.32	28.10	35.50	23.86	61.48	33.56	10.43	40.67
9H-3, 66–67	74.67	83.31	83.31	47.70	43.02	45.79	30.91	21.84	21.39	35.93
9H-5, 66–67	77.67	86.30	86.30	73.80	85.31	73.74	15.27	15.33	10.93	6.43
9H-7, 32–34	80.33	88.97	88.97	87.60	94.62	82.15	7.68	10.47	4.72	4.67
10H-2, 70–71	82.71	93.34	93.34	85.40	92.56	72.38	9.08	15.64	5.52	11.44
11H-2, 70–71	92.21	105.71	105.71	82.60	87.12	71.05	8.30	16.75	9.10	8.04
11H-4, 70–71	95.21	108.71	108.71	69.80	80.22	70.49	25.09	17.06	5.11	12.38
11H-6, 70–71	98.21	111.71	111.71	80.50	86.04	76.49	13.19	11.81	6.31	3.21
12H-1, 65–66	100.16	113.67	113.67	69.30	65.88	64.83	21.08	26.25	9.62	8.30
12H-6, 65–66	107.66	121.18	121.18	56.80	63.80	65.92	26.32	25.85	16.88	11.16
13H-4, 100–102	114.51	128.31	128.31	84.60	86.80	77.32	10.44	11.48	4.96	10.17
15H-5, 0–5	134.03	149.02	149.02	78.40	88.40	84.77	15.06	9.70	6.54	7.61
18H-5, 0–5	162.53	179.57	179.57	82.90	95.07	86.41	12.21	9.90	4.89	8.30
19H-2, 100–102	168.51	185.72	185.72	86.10	94.53	90.81	8.74	6.71	5.16	6.29
20H-2, 100–102	178.01	196.65	196.65	74.60	93.36	72.73	19.24	18.16	6.16	9.40
138-845A-										
1H-3, 40–42	3.41	3.42	3.42	2.92	2.98	7.02	30.46	34.14	66.62	63.65
1H-5, 22–24	6.23	6.22	6.22	2.92	–14.26	3.15	28.49	29.30	68.59	63.64
2H-2, 40–42	9.51	10.40	10.40	3.42	9.13	10.43	31.96	29.76	64.62	54.85
2H-4, 40–42	12.51	13.37	13.37	3.33	26.94	16.31	34.65	29.81	62.02	49.94
2H-6, 101–103	16.12	17.00	17.00	1.67	42.66	15.61	34.99	29.38	63.34	49.30
3H-2, 40–42	19.01	19.88	19.88	2.25	11.84	14.89	39.20	29.21	58.55	45.37
3H-4, 40–42	22.01	22.88	22.88	6.75	14.79	17.50	23.63	26.70	69.62	49.91
3H-6, 40–42	25.01	25.88	25.88	2.42	17.69	5.65	32.81	26.70	64.77	64.93
4H-1, 40–42	27.01	29.15	29.15	8.17	11.48	19.02	28.12	28.37	63.71	47.45
4H-3, 40–42	30.01	32.15	32.15	1.08	23.36	14.82	29.24	26.76	69.68	49.41
4H-5, 101–103	33.62	35.75	35.75	1.42	26.07	2.31	23.49	25.19	75.09	67.07
4H-7, 40–42	36.01	38.15	38.15	3.25	17.21	–0.21	10.40	24.89	86.35	67.90
5H-2, 100–102	38.61	42.13	42.13	2.50	25.87	6.52	27.00	25.30	70.50	63.29
5H-4, 100–102	41.61	45.13	45.13	8.08	16.97	9.69	21.39	27.61	70.53	55.37
6H-1, 30–32	45.91	49.98	49.98	0.33	25.57	12.77	30.63	27.16	69.04	54.39
6H-6, 145–150	54.58	58.64	58.64	0.92	22.34	14.80	18.87	25.69	80.21	59.72
9H-6, 101–103	82.62	90.63	90.63	15.50	35.08	17.64	17.92	23.64	66.58	58.92
10H-2, 101–103	86.12	94.60	94.60	10.92	18.06	5.41	19.92	25.90	69.16	63.03
10H-4, 100–102	89.11	97.60	97.60	4.25	–1.06	6.64	21.90	23.78	73.85	68.27
10H-6, 100–102	92.11	100.60	100.60	26.71	17.80	19.55	18.02	22.09	55.27	62.38
11H-3, 100–102	97.11	106.88	106.88	0.17	17.59	–2.88	10.00	23.33	89.83	67.10
11H-5, 100–102	100.11	109.88	109.88	13.67	8.20	10.59	38.01	24.59	48.32	61.17
12H-1, 100–102	103.61	114.95	114.95	12.92	8.04	4.10	32.33	24.13	54.75	66.79
12H-3, 100–102	106.61	117.92	117.92	21.67	23.08	8.93	34.99	24.40	43.34	56.95
12H-5, 100–102	109.61	120.95	120.95	16.00	1.29	1.70	28.93	24.53	55.07	66.70
13H-1, 100–102	113.11	125.72	125.72	12.17	1.13	1.22	15.50	23.59	72.33	69.59
13H-3, 100–102	116.11	128.73	128.73	0.25	4.26	–0.47	25.02	22.33	74.73	68.17
13H-6, 100–102	120.61	133.23	133.23	0.25	16.58	–0.28	30.02	22.52	69.73	69.71
14H-3, 100–102	125.61	139.60	139.60	0.50	22.29	–0.65	17.10	20.58	82.40	74.89
14H-5, 100–102	128.61	142.60	142.60	0.42	10.08	0.51	26.66	20.03	72.92	76.92
15H-1, 108–110	132.19	148.06	148.06	0.42	6.75	–1.57	11.32	20.29	88.26	83.88
15H-4, 108–110	136.69	152.56	152.56	2.42	27.54	30.94	33.01	32.86	64.57	23.79
15H-6, 108–110	139.69	155.56	155.56	21.42	21.71	25.31	17.37	32.86	61.21	41.21
16H-2, 110–112	143.21	160.93	160.93	67.84	58.82	40.41	8.91	33.26	23.25	41.28
16H-4, 110–112	146.21	163.93	163.93	46.42	18.49	37.19	16.97	27.02	36.61	39.18
16H-6, 110–112	149.21	166.93	166.93	38.63	35.20	51.02	17.03	21.37	44.34	28.11
17H-2, 101–103	152.62	171.43	171.43	80.17	73.16	78.01	5.68	4.03	14.15	14.88
17H-4, 101–103	155.62	174.43	174.43	63.84	60.48	64.42	10.47	8.80	25.69	26.15
17H-6, 101–103	158.62	177.43	177.43	77.34	67.95	71.76	4.66	7.28	18.00	26.93
18H-2, 100–102	162.11	181.40	181.40	74.59	56.16	66.23	5.78	9.89	19.63	29.39
18H-5, 100–102	166.61	185.90	185.90	75.59	67.75	75.77	5.03	7.67	19.38	17.95
19H-1, 101–103	170.12	190.78	190.78	68.51	53.76	63.49	10.85	12.08	20.64	24.05
19H-3, 99–101	173.10	193.74	193.74	85.42	75.79	95.55	2.62	5.19	11.96	–0.85
19H-5, 101–103	176.12	196.78	196.78	83.17	82.50	88.05	6.05	7.97	10.78	2.31
20H-1, 103–105	179.64	201.97	201.97	82.59	67.41	66.25	8.53	12.86	8.88	22.26
20H-3, 100–102	182.61	204.95	204.95	79.17	82.38	79.15	9.96	11.13	10.87	11.84
20H-5, 100–102	185.61	207.95	207.95	74.34	79.78	67.13	8.09	12.33	17.57	25.92
21H-1, 102–104	189.13	212.35	212.35	75.92	76.92	85.01	8.13	8.42	15.95	9.15
21H-3, 99–101	192.10	215.31	215.31	75.42	65.26	73.83	13.70	12.22	10.88	15.00
21H-5, 100–102	195.11	218.35	218.35	79.59	76.79	72.72	8.70	11.85	11.71	16.51

Table 2 (continued).

Core, section, interval (cm)	Depth (mbsf)	Depth (mcd)	Depth (rmcd)	$CaCO_3$ (% measured)	$CaCO_3$ (% estimated from GRAPE density)	$CaCO_3$ (% estimated from reflectance)	Opal (% measured)	Opal (% estimated from reflectance)	Nonbiogenic (% measured)	Nonbiogenic (% estimated from reflectance)
22H-1, 101–103	198.62	223.85	223.85	83.09	75.23	77.28	7.24	10.88	9.67	13.49
22H-3, 102–104	201.63	226.85	226.85	89.76	88.40	90.41	3.71	7.43	6.53	2.26
22H-5, 100–102	204.61	229.85	229.85	86.76	71.93	84.12	7.00	8.99	6.24	8.25
138-846B-										
1H-1, 104–106	1.05	1.06	1.06	60.71	44.17	50.87	33.52	50.68	5.77	8.86
1H-3, 104–106	4.05	4.08	4.10	29.50	25.57	43.63	52.53	33.84	17.97	20.81
1H-5, 65–67	6.66	6.45	6.33	58.67	36.38	55.67	37.09	36.72	4.24	9.04
2H-2, 103–105	9.54	10.22	10.28	57.25	53.17	64.88	36.28	28.16	6.47	11.74
2H-4, 109–111	12.60	13.22	13.24	72.17	63.40	59.90	22.58	35.28	5.25	11.86
2H-6, 103–105	15.54	16.24	16.35	76.59	70.55	59.34	19.72	36.97	3.69	4.35
3H-1, 104–106	17.55	19.60	19.58	73.59	75.32	69.55	19.11	26.46	7.30	6.44
3H-3, 104–106	20.55	22.76	22.89	53.84	55.00	41.77	32.81	34.19	13.35	24.09
3H-5, 104–106	23.55	25.62	25.62	64.76	64.99	58.37	27.30	35.28	7.94	5.05
4H-1, 103–105	27.04	30.20	30.22	50.25	45.66	61.40	48.52	36.21	1.23	4.51
4H-5, 103–105	33.04	36.06	35.98	53.67	66.58	55.42	20.09	30.31	26.24	12.39
5H-1, 104–106	36.55	41.86	41.97	46.92	37.85	59.88	42.33	30.10	10.75	10.35
5H-3, 104–106	39.55	44.66	44.55	37.34	52.19	38.39	45.05	32.39	17.61	26.89
5H-5, 104–106	42.55	47.71	47.68	58.67	66.32	47.43	33.97	36.53	7.36	20.29
6H-1, 104–106	46.05	52.56	52.56	54.92	47.38	62.45	36.79	27.68	8.29	2.81
6H-5, 103–105	52.04	58.52	58.52	32.75	42.34	26.46	61.45	30.43	5.81	35.19
7H-1, 113–105	55.64	63.79	63.64	48.00	47.05	37.16	43.42	33.42	8.58	28.54
7H-3, 104–106	58.55	66.85	66.84	32.25	34.40	21.64	58.30	36.26	9.44	36.09
7H-5, 103–105	61.54	69.82	69.82	14.42	26.05	19.00	75.34	36.73	10.24	34.72
7H-7, 38–40	63.89	72.42	72.64	33.25	31.50	28.37	65.31	38.35	1.44	27.07
8H-2, 38–40	65.89	75.53	75.51	35.59	34.11	34.54	63.61	38.04	0.80	21.84
8H-6, 90–92	72.41	81.98	81.88	65.34	63.63	48.28	29.78	40.44	4.88	4.23
9H-3, 104–106	77.55	87.60	87.46	56.17	59.53	51.98	32.84	32.07	10.99	13.65
9H-5, 104–106	80.55	90.70	90.69	65.92	65.29	49.72	24.85	36.59	9.23	7.53
10H-1, 107–109	84.08	97.00	97.25	45.17	41.18	43.93	42.23	44.09	12.60	13.34
10H-3, 108–100	87.09	99.67	99.67	45.67	52.86	60.26	43.01	29.66	11.32	15.34
10H-5, 118–100	90.19	102.71	102.69	47.00	54.95	49.43	47.63	37.20	5.37	12.97
11H-1, 97–99	93.48	107.16	107.32	37.09	38.30	41.07	58.38	54.42	4.53	7.74
11H-3, 103–105	96.54	110.34	110.66	65.92	79.38	67.80	18.12	17.86	15.96	7.22
11H-5, 103–105	99.54	113.22	113.41	53.92	64.77	61.81	36.52	27.23	9.56	8.24
12H-1, 103–105	103.04	117.89	117.97	56.42	60.80	69.21	33.05	18.28	10.53	8.58
12H-3, 103–105	106.04	120.87	120.93	45.50	60.71	60.00	44.44	30.97	10.06	4.23
12H-5, 103–105	109.04	123.83	123.84	42.50	58.59	48.68	37.64	29.47	19.86	17.49
13H-1, 102–104	112.53	129.26	129.40	50.17	49.78	63.78	41.28	25.84	8.55	8.69
13H-3, 101–103	115.52	131.87	131.76	30.00	40.04	36.53	49.12	44.94	20.87	14.99
13H-5, 103–105	118.54	135.36	135.86	57.34	69.66	56.84	30.60	33.68	12.06	5.34
14H-1, 102–104	122.03	139.40	139.66	68.84	77.46	79.34	16.83	18.48	14.33	9.43
14H-3, 103–105	125.04	142.33	142.47	72.01	78.80	73.48	16.59	20.21	11.40	–0.49
14H-5, 135–107	128.36	145.58	145.70	53.17	60.05	61.55	36.52	32.31	10.31	6.90
15H-2, 124–106	133.25	152.96	152.96	34.42	57.86	40.58	43.15	29.46	22.43	32.49
15H-4, 103–105	136.04	155.84	155.94	36.84	48.99	50.76	53.81	41.08	9.34	14.83
15H-6, 104–106	139.05	158.81	158.85	58.09	69.14	52.68	22.75	28.13	19.16	17.53
16H-2, 102–104	142.53	162.78	162.83	78.17	81.11	74.40	12.89	18.57	8.94	11.22
16H-5, 102–104	147.03	167.18	167.15	76.67	81.03	76.28	11.36	19.03	11.97	5.10
17H-1, 102–104	150.53	171.78	171.80	71.34	76.85	74.24	15.50	19.21	13.16	4.57
17H-3, 102–104	153.53	174.76	174.75	67.05	65.16	58.27	27.06	27.47	5.89	8.87
17H-5, 104–106	156.55	177.91	178.01	44.21	65.08	59.20	46.58	32.81	9.21	8.11
18H-1, 110–102	160.11	181.63	181.32	61.92	59.12	71.41	28.08	20.88	10.00	6.90
18H-3, 102–104	163.03	184.92	184.96	84.59	93.17	83.84	8.81	10.44	6.60	6.21
18H-5, 102–104	166.03	187.86	187.85	84.51	88.32	71.69	9.69	7.75	5.80	23.98
19H-1, 103–105	169.54	193.39	193.49	78.26	81.87	70.39	12.89	20.58	8.85	4.27
19H-3, 103–105	172.54	196.32	196.32	71.84	81.82	67.12	10.40	27.39	17.76	2.36
19H-5, 103–105	175.54	199.32	199.32	81.09	87.27	75.22	11.02	18.86	7.89	3.75
20H-2, 103–105	180.54	206.09	206.08	77.92	87.20	68.56	11.97	23.54	10.11	4.51
20H-4, 103–105	183.54	209.16	209.19	71.26	71.43	70.41	19.55	19.53	9.19	7.77
20H-6, 103–105	186.54	212.07	212.01	76.09	80.27	75.91	13.40	16.93	10.51	5.02
21H-2, 103–105	190.04	216.97	216.97	69.01	72.91	66.32	25.09	31.02	5.90	1.08
21H-4, 103–105	193.04	219.97	219.97	72.67	81.44	69.73	17.17	21.86	10.16	8.75
21H-6, 103–105	196.04	222.96	222.95	73.42	87.92	76.38	16.83	20.71	9.75	7.51
22H-2, 103–105	199.54	229.99	230.00	68.34	74.27	72.98	20.67	20.57	10.99	4.55
22H-4, 103–105	202.54	232.97	232.97	63.59	63.82	73.83	28.08	21.46	8.33	3.97
22H-6, 103–105	205.54	235.99	236.02	51.84	65.62	70.60	40.83	21.91	7.33	5.48
138-847B-										
1H-2, 102–104	2.53	2.52	2.52	39.00	24.91	40.49	41.00	21.35	20.00	33.33
1H-4, 103–105	5.54	5.66	5.76	54.17	48.17	63.21	32.57	18.71	13.26	13.68
2H-1, 103–105	7.54	7.64	7.63	50.17	61.09	75.36	30.67	17.37	19.16	5.12
2H-3, 32–34	9.83	9.97	9.97	76.55	64.90	73.03	10.27	17.85	13.18	2.62
2H-5, 107–109	13.58	13.69	13.69	79.59	79.36	77.40	13.26	12.00	7.15	4.77
2H-7, 14–16	15.65	15.66	15.58	66.51	54.60	69.32	12.65	12.83	20.84	14.82
3H-3, 102–104	20.03	20.35	20.33	80.09	76.39	70.40	12.38	19.39	7.53	7.90
3H-5, 102–104	23.03	23.35	23.33	48.21	62.61	52.56	19.45	18.82	32.34	24.60
3H-7, 33–35	25.34	25.57	25.43	58.00	47.50	69.84	20.16	13.58	21.84	12.60
4H-2, 102–104	28.03	30.85	30.85	73.76	58.46	62.02	24.21	17.80	2.03	16.49
4H-4, 102–104	31.03	33.65	33.56	58.34	62.38	54.56	22.17	22.63	19.49	17.79
4H-6, 102–104	34.03	36.92	37.01	62.25	64.22	67.83	15.44	13.89	22.31	16.08
5H-1, 133–105	36.34	39.14	39.14	69.34	66.03	73.62	13.91	15.17	16.75	5.25
5H-3, 104–106	39.05	41.86	41.86	52.25	44.63	58.50	40.29	17.93	7.46	19.78
5H-7, 49–51	44.50	47.30	47.30	57.34	57.96	66.49	33.46	19.61	9.20	9.37
6H-2, 103–105	47.04	52.00	51.91	51.50	41.89	37.08	33.97	29.61	14.53	26.06
6H-4, 32–34	49.33	54.32	54.23	25.29	20.05	13.78	45.66	26.36	29.05	50.95
6H-6, 104–106	53.05	58.23	58.34	30.50	44.14	18.10	32.95	27.91	36.55	45.44
7H-1, 103–105	55.04	61.78	61.77	52.75	44.07	41.58	30.12	27.45	17.13	25.09

Table 2 (continued).

Core, section, interval (cm)	Depth (mbsf)	Depth (mcd)	Depth (rmcd)	$CaCO_3$ (% measured)	$CaCO_3$ (% estimated from GRAPE density)	$CaCO_3$ (% estimated from reflectance)	Opal (% measured)	Opal (% estimated from reflectance)	Nonbiogenic (% measured)	Nonbiogenic (% estimated from reflectance)
7H-3, 103–105	58.04	64.63	64.46	26.59	31.05	10.02	50.25	28.95	23.16	51.13
7H-5, 103–105	61.04	67.45	67.15	59.00	59.52	61.84	31.45	20.78	9.55	13.82
7H-7, 37–39	63.38	70.13	70.13	68.34	72.28	57.86	21.22	19.33	10.44	18.07
8H-2, 103–105	66.04	74.13	74.07	69.09	68.83	67.37	19.48	22.71	11.43	4.10
8H-4, 103–105	69.04	77.26	77.31	60.17	57.21	64.14	25.91	16.97	13.92	16.46
8H-6, 100–102	72.01	80.39	80.59	73.34	78.16	82.76	16.42	10.35	10.24	4.18
9H-2, 26–28	74.77	84.20	84.15	40.78	40.89	44.80	44.68	25.88	14.54	22.06
9H-4, 103–105	78.54	87.87	87.71	77.17	68.51	53.25	12.44	21.84	10.39	17.87
9H-6, 97–99	81.48	91.00	91.03	70.51	77.96	75.40	16.76	15.38	12.73	2.86
10H-2, 109–110	85.10	95.11	94.97	67.34	62.79	56.85	14.69	17.46	17.97	20.82
10H-4, 104–106	88.05	98.29	98.29	74.59	81.82	76.21	16.05	12.79	9.36	7.52
10H-6, 102–104	91.03	101.25	101.25	66.51	66.39	65.51	19.52	16.43	13.97	11.83
11H-1, 32–34	92.33	105.02	104.84	61.25	62.58	63.97	24.11	19.07	14.64	8.20
11H-3, 32–34	95.33	108.13	108.04	62.42	68.08	65.10	23.80	18.11	13.78	9.36
11H-5, 34–36	98.35	111.20	111.15	68.01	76.15	72.98	14.45	12.20	17.54	10.96
12H-1, 33–35	101.84	114.82	114.76	72.67	64.24	66.63	13.60	15.88	13.73	12.01
12H-3, 33–35	104.84	117.78	117.70	65.17	64.15	48.67	18.33	19.46	16.50	24.51
12H-5, 33–35	107.84	120.74	120.66	67.09	64.07	64.80	17.68	15.56	15.23	16.65
12H-7, 44–46	110.95	124.05	124.10	76.01	82.63	67.12	12.24	17.54	11.75	12.05
13H-2, 33–35	112.84	126.85	126.86	68.34	63.93	43.83	18.67	23.21	12.99	26.32
13H-4, 33–35	115.84	129.87	129.90	81.51	81.30	70.80	8.60	11.50	9.89	14.65
13H-6, 33–35	118.84	132.86	132.88	65.17	70.93	40.98	15.27	18.33	19.56	38.25
14H-1, 33–35	120.84	136.41	136.50	74.13	83.64	81.26	8.53	9.10	17.34	5.82
14H-3, 33–35	123.84	139.26	139.18	74.67	81.15	77.06	14.21	12.90	11.12	5.91
14H-5, 102–104	127.53	143.04	143.09	42.92	53.23	55.51	43.66	25.26	13.42	15.77
14H-7, 33–35	129.84	145.30	145.29	61.09	75.46	65.93	28.90	23.61	10.01	9.95
15H-2, 33–35	131.84	146.15	145.61	56.21	67.12	65.18	30.97	25.02	12.82	8.48
15H-5, 33–35	136.34	147.66	146.11	46.00	50.71	54.19	41.39	35.70	12.61	13.07
15H-7, 33–35	139.34	148.66	146.44	31.79	57.17	48.12	49.47	26.90	18.74	18.98

chosen to exclude disturbed intervals around sediment biscuits, the estimates of $CaCO_3$ percentage from GRAPE were more precise (RMS error ±11.8%, $r^2 = 0.74$) than the estimates from reflectance (RMS error ±14.3%, $r^2 = 0.62$). Note that the GRAPE estimates include corrections for downhole compaction and porosity rebound. The reflectance estimates were calibrated only with unlithified samples from APC cores and contain no corrections for compaction. We conclude that errors in reflectance associated either with surface roughness or with lithification in XCB cores degrade the predictions of lithology slightly. Improvements may come from (1) calibrating equations to predict lithologies from reflectance in partially lithified materials separately from unlithified materials, (2) improving methods of splitting partially lithified sediment cores to minimize surface roughness, or (3) reducing the sensitivity to surface roughness by measuring diffuse, rather than directional, reflectance.

To further check the fidelity of the two estimates of $CaCO_3$ concentration within the APC cores, we compare the statistical properties of the reflectance and GRAPE estimates in Site 846, over the same time series represented in Figure 7. The distribution of variance in this time series is essentially identical for reflectance and GRAPE estimates. The power spectra demonstrate that both estimators have similar distributions of variance over the last 3.5 Ma, with significant concentrations in the primary earth orbital bands of 41, 23, and 19 k.y. and at long periods (Fig. 9A). The two time series are significantly coherent (Fig. 9B) and in phase (Fig. 9C) in essentially all bands in which the data variance is large.

The horizontal dashed line in Figure 9A represents the noise level in calibration of $CaCO_3$ percentages based on GRAPE density. The noise level for the reflectance estimate would be slightly lower. This calculation of noise level in variance density units assumes that misfits are random (white) noise that can be represented by the total variance (σ^2) times the fraction of variance left unexplained ($1 - r^2$), divided by the bandwidth of this analysis (0.0012 k.y.$^{-1}$). Where variance in the time series of the GRAPE and reflectance estimates of $CaCO_3$ concentration drops below that expected for noise in the calibration (at high frequencies), the two calcium carbonate estimates are not coherent, and we cannot assume that either is a good estimate of true concentration of $CaCO_3$. The strong coherency of the two estimates at longer periods, however, indicates that both are recording similar lithologic variations for the frequency bands in which the variance is strong. Because the assumptions behind the GRAPE and reflectance methods are completely different, we concluded that both are good measures of the history of $CaCO_3$ concentration in the eastern tropical Pacific Ocean.

SUMMARY AND CONCLUSIONS

Reflectance spectroscopy has great potential for providing long, high-resolution time series of lithologic proxy measurements at a precision sufficient for many studies of marine geologic history. The technique can be used to scan unprepared core surfaces. It is rapid enough that large data sets can be produced at sea as cores are recovered and opened. Quantitative estimates of lithology can be calibrated with reasonably small ground-truth data sets generated by traditional chemical methods. This technique is efficient in both cost and materials, as it works well with automation, minimizes labor-intensive chemical measurements, and preserves material for other measurements that must consume sediment.

Reflectance measurements performed during Leg 138 were calibrated here to estimate quantitatively the concentrations of $CaCO_3$, opal, and nonbiogenic sediment components in the eastern tropical Pacific Ocean. The equations calibrated here are not universal, but are applicable within the geologic setting of the eastern Pacific. Estimates of $CaCO_3$ percentage from reflectance spectra are robust over a large range, with RMS errors of about 9%. This precision is as good or better than carbonate estimates based on GRAPE density measurements, in environments having a significant nonbiogenic component. Reflectance spectroscopy will be especially useful in these environments. Estimates of the concentration of nonbiogenic sediment are usually reasonable, but not as successful as the estimates of $CaCO_3$ percentage. Mismatches between the estimates of nonbiogenic sediment made by reflectance and chemical measurements may point to variations in the mineralogy of the nonbiogenic sediment that warrant further study. Estimates of opal concentration may work reasonably well at low opal concentrations, but are poorly constrained at high concentrations.

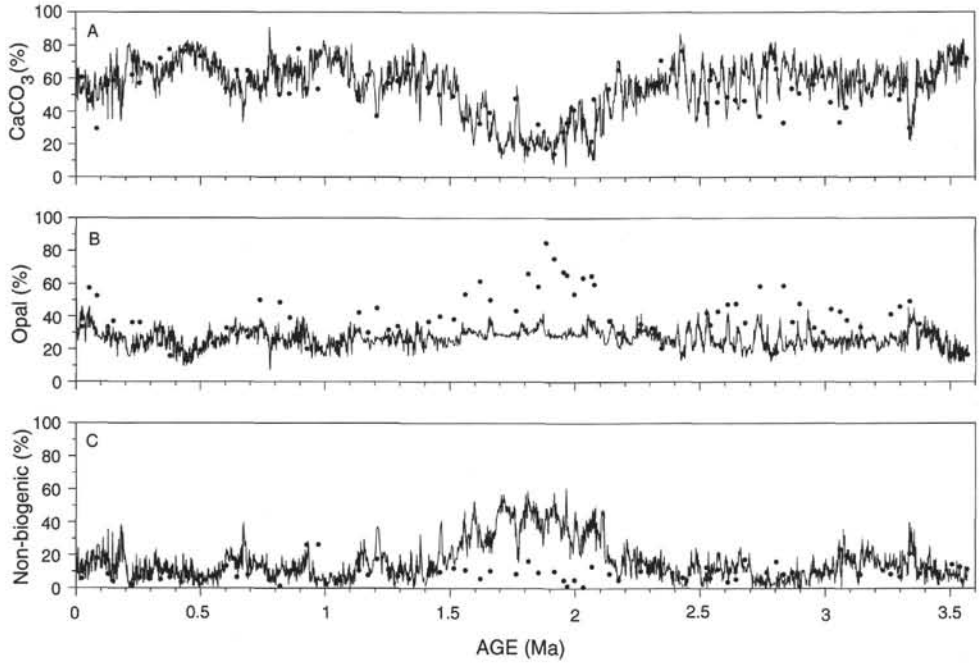

Figure 7. Time series reconstructions of sedimentary components at Site 846, estimated from reflectance spectra. **A.** $CaCO_3$%. **B.** Opal%. **C.** Nonbiogenic sediment%. Estimated $CaCO_3$ and nonbiogenic sediment percentages are strongly negatively correlated (r = –0.95). Estimated opal is weakly correlated to nonbiogenic sediment percentages (r = +0.61). Solid circles are discrete ground-truth samples measured chemically. In **B**, reflectance often underestimates high opal concentrations, producing a signal of artificially low amplitude. In **C**, the estimates of nonbiogenic sediment are generally good, but overestimate values from 1.5 to 2.1 Ma.

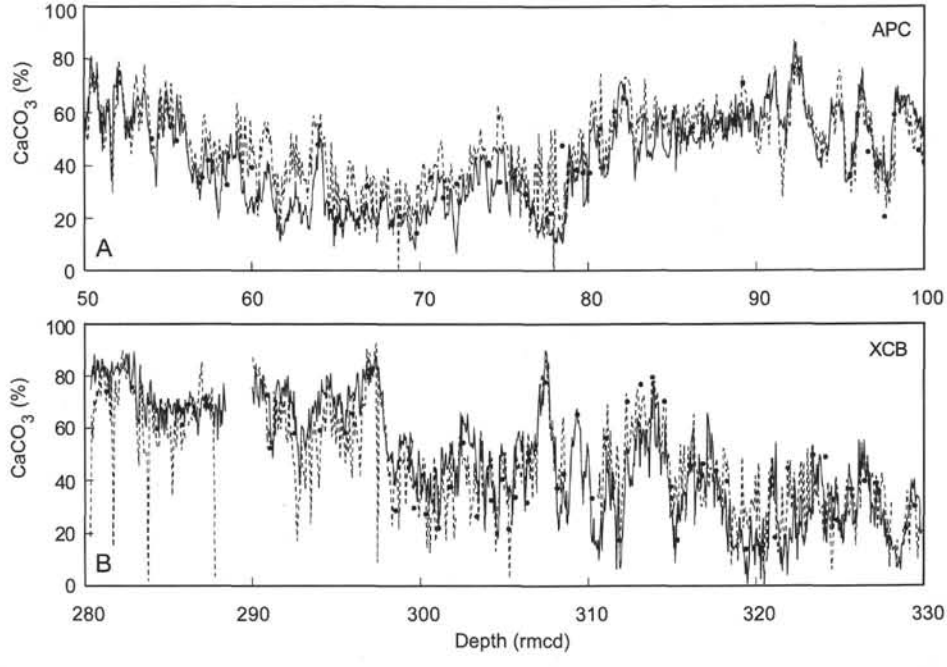

Figure 8. Percentages of $CaCO_3$ from Site 846, comparing estimates from reflectance spectra (solid line), from GRAPE density (dashed line), and from discrete chemical measurements (solid points) in typical intervals of APC and XCB cores. **A.** Example of APC cores from Holes 846B, 846C, and 846D, plotted as a complete record from depths of 50 to 100 rmcd in the "shipboard splice," a composite record that fills gaps between cores with complete intervals from adjacent holes (Hagelberg et al., 1992). The sample interval for the reflectance and GRAPE estimates is 4 cm. **B.** Example of XCB cores from Hole 846B, from depths of 280–330 rmcd. No attempt was made to create a composite section by combining data from multiple holes at these depths. The sample interval for reflectance measurements was 8 cm. GRAPE data were interpolated to 8-cm intervals at approximately the same sample depths as the reflectance data. Note the low spikes in GRAPE density estimates of $CaCO_3$ percentage in the XCB interval. These are probably an artifact of GRAPE density measurements, including disturbed, water-saturated material around oblong sediment "biscuits," common in XCB cores. Reflectance estimates, measured along the axis of the cores where biscuits tend to meet, are not sensitive to this error and thus may yield a better estimate of lithology in materials recovered by XCB.

Table 3. Measured and estimated $CaCO_3$ percentages in XCB cores.

Core, section, interval (cm)	Depth (mbsf)	$CaCO_3$ (% measured)	$CaCO_3$ (%)[a]	$CaCO_3$ (%)[b]
138-844B-				
21X-6, 100–102	193.51	74.30	70.54	43.16
30X-2, 107–109	274.18	72.80	85.41	39.98
30X-4, 82–84	267.93	56.60	76.52	45.95
30X-6, 106–108	280.17	64.30	80.60	44.89
31X-2, 125–127	283.96	51.30	62.76	28.59
138-846B-				
23X-1, 103–105	207.54	71.59	67.38	59.91
23X-2, 103–105	209.04	68.17	78.48	68.31
23X-3, 103–105	210.54	73.26	77.03	63.11
23X-4, 103–105	212.04	73.51	78.42	77.20
23X-5, 103–105	213.54	64.67	76.97	68.59
23X-6, 103–105	215.04	75.42	88.57	69.73
24X-1, 102–104	217.23	84.42	91.59	79.97
24X-2, 102–104	218.73	79.26	93.70	76.72
24X-3, 102–104	220.23	82.92	86.62	72.52
24X-4, 102–104	221.73	70.17	79.59	73.25
24X-5, 102–104	223.23	67.92	86.58	69.29
24X-6, 102–104	224.73	76.26	86.56	65.71
25X-1, 102–104	226.73	61.34	38.53	65.34
25X-2, 103–105	228.24	66.09	61.16	78.51
25X-3, 103–105	229.74	67.59	68.59	59.49
25X-4, 103–105	231.24	75.59	79.40	72.05
27X-1, 103–105	246.24	74.09	58.63	75.85
27X-2, 103–105	247.74	75.67	81.69	65.00
27X-3, 103–105	249.24	59.75	62.53	63.89
27X-4, 103–105	250.74	61.17	58.49	58.65
27X-5, 103–105	252.24	68.26	62.45	64.38
28X-1, 103–105	255.94	52.42	54.11	67.41
28X-2, 101–103	257.42	58.00	47.27	54.00
28X-3, 102–104	258.93	59.09	51.81	57.99
28X-4, 103–105	260.44	58.00	56.12	59.12
28X-5, 103–105	261.94	82.51	82.66	81.36
28X-6, 103–105	263.44	28.71	23.56	35.30
29X-1, 103–105	265.24	27.42	26.33	34.96
29X-2, 102–104	266.73	37.67	51.56	46.93
29X-3, 108–110	268.29	26.50	37.02	35.85
29X-4, 104–106	269.75	40.59	53.68	48.87
29X-5, 102–104	271.23	31.75	46.81	41.92
29X-6, 63–65	272.34	77.80	77.18	76.55
29X-7, 22–24	273.43	42.59	31.54	30.30
30X-2, 58–60	275.99	56.25	57.75	48.51
30X-2, 135–137	276.76	17.50	28.67	3.81
30X-3, 112–114	278.03	76.76	67.35	49.55
30X-4, 102–104	279.43	70.17	61.69	42.64
30X-5, 104–106	280.95	45.42	55.49	37.89
30X-6, 106–108	282.47	43.67	51.06	37.69
30X-7, 23–25	283.14	39.75	25.63	19.23
31X-1, 79–81	284.30	14.08	25.58	7.04
31X-2, 103–105	286.04	18.42	38.95	45.10
31X-3, 103–105	287.54	23.34	57.41	31.47
31X-4, 101–103	289.02	48.92	25.39	31.71
31X-5, 103–105	290.54	36.67	38.78	33.55
31X-6, 103–105	292.04	38.92	41.25	27.76
32X-2, 103–105	295.64	24.42	16.36	10.29
32X-3, 106–108	297.17	9.75	7.00	10.65
32X-4, 105–107	298.66	7.83	22.14	10.40
32X-5, 106–108	300.17	5.92	–2.94	–4.18
32X-6, 96–98	301.57	34.00	27.71	32.28
33X-1, 103–105	303.84	22.25	38.31	37.11
34X-3, 123–125	316.64	50.09	49.96	36.00
34X-4, 113–115	318.04	33.09	42.82	35.42
34X-5, 33–35	318.74	59.00	62.55	59.22
34X-7, 23–25	321.64	68.26	66.23	59.89
35X-4, 119–121	327.70	64.76	74.50	58.00
35X-5, 114–116	329.15	55.92	60.29	39.34
35X-6, 114–116	330.65	67.92	71.23	62.36
36X-1, 108–110	332.79	65.01	62.16	31.29
36X-2, 130–132	334.51	72.92	49.39	58.52
36X-3, 130–132	336.01	66.01	72.74	57.43
36X-4, 122–124	337.43	74.17	72.70	64.97
36X-6, 105–107	340.26	63.51	49.20	55.08
37X-2, 95–97	343.76	85.09	84.74	73.43
38X-1, 98–100	351.99	62.25	55.48	68.49
38X-5, 114–116	358.15	67.34	48.62	69.41
40X-1, 123–125	371.54	79.42	83.15	48.22
40X-2, 103–105	372.84	84.26	92.03	53.62
40X-3, 105–107	374.36	69.92	89.95	44.61
40X-4, 88–90	375.69	73.51	92.58	40.13
40X-5, 120–122	377.51	71.01	70.11	36.13
41X-1, 102–104	380.93	90.63	82.99	78.43
41X-3, 115–117	384.06	88.13	69.95	64.48
41X-4, 82–84	385.23	81.34	69.93	67.79
42X-1, 91–93	390.52	78.59	83.99	56.19
44X-2, 130–132	411.71	75.59	93.33	24.71
44X-4, 94–96	414.35	66.17	72.56	35.88
138-847B-				
22X-5, 33–35	199.54	71.92	87.65	73.81
22X-6, 32–34	201.03	56.59	73.86	62.82
22X-7, 23–25	202.44	71.09	83.41	73.43
23X-1, 31–33	203.12	83.09	86.64	86.86
23X-2, 32–34	204.63	74.34	80.92	72.02
23X-3, 31–33	206.12	76.92	86.59	72.71
23X-4, 32–34	207.63	75.26	91.52	69.15
23X-5, 32–34	209.13	67.17	86.55	70.27
23X-6, 33–35	210.64	59.75	27.82	64.56
23X-7, 22–24	212.03	72.76	91.48	68.27
24X-1, 32–34	212.83	69.09	87.47	75.28
24X-2, 32–34	214.33	75.26	80.73	79.00
24X-3, 32–34	215.83	72.84	75.07	65.62
24X-4, 32–34	217.33	81.59	86.43	82.98
24X-5, 33–35	218.84	84.76	94.00	79.67
24X-6, 32–34	220.33	67.01	84.25	76.40
25X-1, 32–34	222.53	85.17	92.01	84.19
25X-2, 32–34	224.03	67.17	73.33	67.96
25X-3, 30–32	225.51	75.67	80.52	71.63
25X-4, 41–43	227.12	64.34	71.64	62.74
25X-5, 38–40	228.59	69.01	74.79	78.54
25X-6, 31–33	230.02	54.67	56.53	63.76
25X-7, 23–25	231.44	57.25	66.33	66.75

[a] Estimated from GRAPE density.
[b] Estimated from reflectance.

The present study of Leg 138 sediments considered reflectance spectra over most of the visible and some of the nIR bands (455–945 nm). The instrument was a first-generation prototype, and many improvements are expected in the future. We think that major improvements will come from (1) expansion of the wavelengths measured to better capture unique mineral reflectance signatures, (2) collection of diffuse, rather than directional, reflectance to minimize the effects of surface roughness, and (3) improvements in array detector technology that will improve the signal/noise ratios and speed up the analyses.

ACKNOWLEDGMENTS

We thank USSAC for funding of instrument development and post-cruise science, and the Leg 138 shipboard party for assistance at sea. This manuscript benefited from helpful reviews by W. Busch, S. O'Connell, and W. Balsam, and editorial comments from L. Mayer.

REFERENCES*

Baker, E.Q., and Louda, J.W., 1986. Porphyrins in the geological record. *In* Johns, R.B. (Ed.) *Biological Markers in the Sedimentary Record:* Amsterdam (Elsevier), 125–225.

Balsam, W.L., 1992. Estimating sediment organic content and percent calcium carbonate in marine sediment from NUV/VIS/NIR spectra. *Eos,* 73:308.

Balsam, W.L., and Deaton, B.C., 1991. Sediment dispersal in the Atlantic Ocean: evaluation by visible light spectra. *Rev. Aquat. Sci.,* 4:411–447.

Barranco, F.T., Jr., Balsam, W.L., and Deaton, B.C., 1989. Quantitative reassessment of brick red lutites: evidence from reflectance spectrophotometry. *Mar. Geol.,* 89:299–314.

*Abbreviations for names of organizations and publications in ODP reference lists follow the style given in *Chemical Abstracts Service Source Index* (published by American Chemical Society).

Boyce, R.E., 1976. Definitions and laboratory techniques of compressional sound velocity parameters and wet-water content, wet-bulk density, and porosity parameters by gravimetric and gamma ray attenuation techniques. *In* Schlanger, S.O., Jackson, E.D., et al., *Init. Repts. DSDP,* 33: Washington (U.S. Govt. Printing Office), 931–958.

Busch, W.H., 1991. Analysis of wet-bulk density and sediment color cycles in Pliocene-Pleistocene sediments of the Owen Ridge (Site 722) and Oman Margin (Site 728). *In* Prell, W.L., Niitsuma, N., et al., *Proc. ODP, Sci. Results,* 117: College Station, TX (Ocean Drilling Program), 239–253.

Clark, R.N., 1981. The spectral reflectance of water-mineral mixtures at low temperatures. *J. Geophys. Res.,* 86:3074–3086.

Clark, R.N., Trude, V., King, V., Klejwa, M., Swayze, G.A., and Vergo, N., 1990. High spectral resolution reflectance spectroscopy of minerals. *J. Geophys. Res.,* 95:12653–12680.

Deaton, B.C., and Balsam, W.L., 1991. Visible spectroscopy: a rapid method for determining hematite and goethite concentrations in geological materials. *J. Sediment. Petrol.,* 61:629–632.

Gaffey, S.J., 1986. Spectral reflectance of carbonate minerals in the visible and near infrared (0.35 to 2.55 μm): calcite, aragonite, and dolomite. *Am. Mineral.,* 71:151–162.

Hagelberg, T., Shackleton, N., Pisias, N., and Shipboard Scientific Party, 1992. Development of composite depth sections for Sites 844 through 854. *In* Mayer, L., Pisias, N., Janecek, T., et al., *Proc. ODP, Init. Repts.,* 138 (Pt. 1): College Station, TX (Ocean Drilling Program), 79–85.

Heath, G.R., Moore, T.C., Jr., and Roberts, G.L., 1974. Mineralogy of surface sediments from the Panama Basin, Eastern Equatorial Pacific. *J. Geol.,* 82:145–160.

Herbert, T.D., and Mayer, L.A., 1991. Long climatic time series from sediment physical property measurements. *J. Sediment. Petrol.,* 61:1089–1108.

Hoffer, R.M., 1984. Remote sensing to measure the distribution and structure of vegetation. *In* Woodwell, G.M. (Ed.), *The Role of Terrestrial Vegetation in the Global Carbon Cycle: Measurement by Remote Sensing:* New York (Wiley), 131–159.

Hunt, G.R., 1977. Spectral signatures of particulate minerals in the visible and near infrared. *Geophysics,* 42:501–513.

Hunt, G.R., and Salisbury, J.W., 1970. Visible and near-infrared spectra of minerals and rocks. I: Silicate minerals. *Mod. Geol.,* 1:283–300.

————, 1971. Visible and near-infrared spectra of minerals and rocks. II: Carbonates. *Mod. Geol.,* 2:23–30.

Hunt, G.R., Salisbury, J.W., and Lenhoff, C.J., 1971a. Visible and near-infrared spectra of minerals and rocks. III: Oxides and hydroxides. *Mod. Geol.,* 2:195–205.

————, 1971b. Visible and near-infrared spectra of minerals and rocks. IV: Sulphides and sulphates. *Mod. Geol.,* 3:1–14.

Lyle, M., 1983. The brown-green color transition in marine sediments: a marker of the Fe(III)-Fe(II) redox boundary. *Limnol. Oceanogr.,* 28:1026–1033.

Mayer, L.A., 1991. Extraction of high-resolution carbonate data for paleoclimate reconstruction. *Nature,* 352:148–150.

Mayer, L.A., Pisias, N.G., Janecek, T.R., et al., 1992. *Proc. ODP, Init. Repts.,* 138 (Pts. 1 and 2): College Station, TX (Ocean Drilling Program).

Mix, A.C., Rugh, W., Pisias, N.G., Veirs, S., Leg 138 Shipboard Sedimentologists (Hagelberg, T., Hovan, S., Kemp, A., Leinen, M., Levitan, M., Ravelo, C.), and Leg 138 Scientific Party, 1992. Color reflectance spectroscopy: a tool for rapid characterization of deep-sea sediments. *In* Mayer, L., Pisias, N., Janecek, T., et al., *Proc. ODP, Init. Repts.,* 138 (Pt. 1): College Station, TX (Ocean Drilling Program), 67–77.

Mortlock, R.A., and Froelich, P.N., 1989. A simple method for the rapid determination of biogenic opal in pelagic marine sediments. *Deep-Sea Res. Part A,* 36:1415–1426.

Schumann, D., and Nagel, U. , 1982. Leg 68: shore-based X-ray mineralogy. *In* Prell, W.L., Gardner, J.V., et al., *Init. Repts. DSDP,* 68: Washington (U.S. Govt. Printing Office), 397–402.

Zimmerman, H.B., 1982. Lithologic stratigraphy and clay mineralogy of the western Caribbean and eastern equatorial Pacific, Leg 68, Deep Sea Drilling Project. *In* Prell, W.L., Gardner, J.V., et al., *Init. Repts. DSDP,* 68: Washington (U.S. Govt. Printing Office), 383–395.

Date of initial receipt: 18 June 1993
Date of acceptance: 8 June 1994
Ms 138SR-121

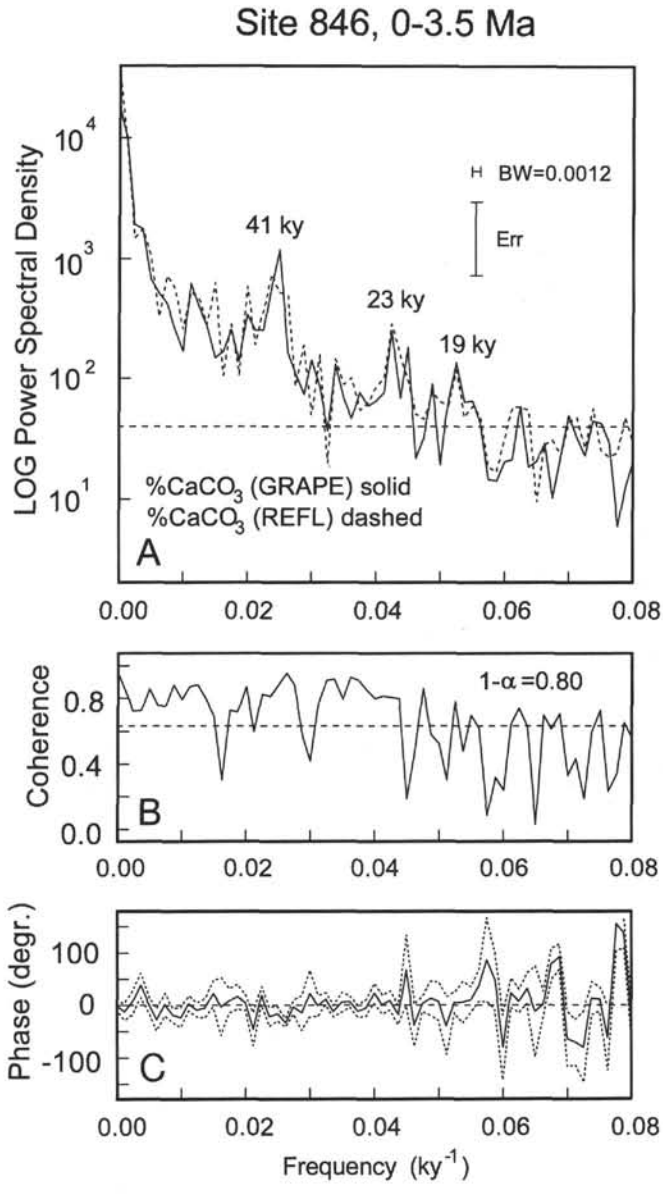

Figure 9. Time series analysis compares the estimates of $CaCO_3$ percentage based on GRAPE density with those based on reflectance spectra over the past 3.5 Ma at Site 846. Bandwidth of this analysis is 0.0012 k.y.$^{-1}$. **A.** Power spectral density as a function of frequency demonstrates a similar distribution of variance in both estimates (GRAPE density is the solid line, reflectance is dashed). The horizontal dashed line is the noise level of the GRAPE calibration, assuming that all variance in the calibration data set for $CaCO_3$ percentage unaccounted for by GRAPE estimates is "white" noise, distributed equally in all frequency bands. **B.** The coherency spectrum between GRAPE and reflectance estimates of $CaCO_3$ indicates that both are linearly correlated with each other, at greater than 80% confidence interval ($1 - \alpha > 0.80$) in essentially all frequency bands that contain significant variance (<0.55 k.y.$^{-1}$). **C.** The phase spectrum between GRAPE and reflectance estimates of $CaCO_3$ indicates that both are in phase with each other, within an error envelope of 80% confidence interval, in essentially all frequency bands that contain significant variance (<0.55 k.y.$^{-1}$).